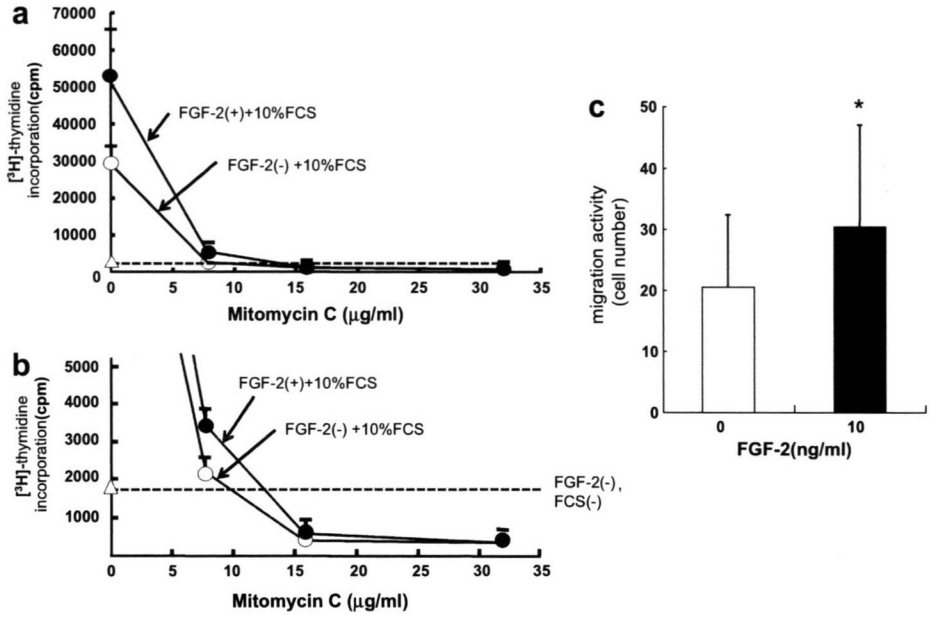

Figure 6. FGF-2 elevated cell migration by HDPC independent of cell proliferation. (*a*) HDPC were cultured with 10% FCS standard medium in 24-well culture plates to confluency and were made quiescent by culturing for 24 hours in a serum-free medium. After treatment with or without MMC for 2 hours, the cells were cultured in the presence (closed circle) or absence (open circle) of FGF-2 (10 ng/mL). HDPC were cultured in the absence of FCS, FGF-2, and MMC as a negative control (open triangle and dotted line). Proliferation was assayed by 4 hours of pulsing in wells by using [^{3}H]-thymidine. [^{3}H]-thymidine incorporation was measured in a liquid scintillation counter. Results of mean and SEM of 3 identical experiments are shown. *$P < .05$. (*b*) In this graph vertical axis is plotted as 0–5000 cpm from (*a*). (*c*) MMC-treated HDPC were seeded on a glass bottom dish, on which was placed a silicon block to introduce a cell-free area, and grown until confluence. The silicon block was then removed, and the medium was replaced with 1% FCS α-MEM in the presence or absence of FGF-2 (10 ng/mL). Migration of HDPC to the cleared area was photographed immediately after removing the silicon block and 24 hours later by using phase contrast. Migratory activity was estimated by the assay described in Materials and Methods. Results of mean and SEM of 3 identical experiments are shown. *$P < .05$.

Acknowledgments

This work was supported by a part of Grants-in-Aid for Scientific Research (no. 20592427) and the 21st Century COE entitled "Organization of Frontier BioDentistry" at Osaka University Graduate School of Dentistry supported by the Ministry of Education, Culture, Sports, Science and Technology.

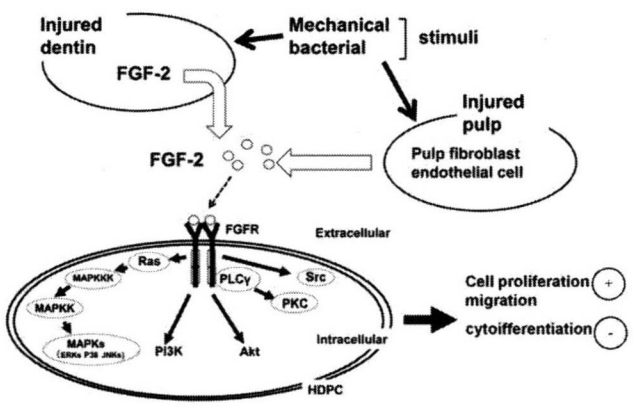

Figure 7. FGF-2 is localized in dentin and released after injury. Also, fibroblasts and endothelial cells in dental pulp produce FGF-2. Thus, HDPC are exposed to FGF-2 in physiologic and pathophysiologic conditions. HDPC expressed FGFR mRNA. FGFRs are activated by its ligands such as FGF-2 and mediate cellular functions of the cells via various signaling pathways.

References

1. Gronthos S, Mankani M, Brahim J, Robey PG, Shi S. Postnatal human dental pulp stem cells (DPSCs) in vitro and in vivo. Proc Natl Acad Sci U S A 2000;97:13625–30.
2. Gronthos S, Brahim J, Li W, et al. Stem cell properties of human dental pulp stem cells. J Dent Res 2002;81:531–5.
3. Batouli S, Miura M, Brahim J, et al. Comparison of stem-cell-mediated osteogenesis and dentinogenesis. J Dent Res 2003;82:976–81.
4. Laino G, d'Aquino R, Graziano A, et al. A new population of human adult dental pulp stem cells: a useful source of living autologous fibrous bone tissue (LAB). J Bone Miner Res 2005;20:1394–402.
5. Kuo MY, Lan WH, Lin SK, Tsai KS, Hahn LJ. Collagen gene expression in human dental pulp cell cultures. Arch Oral Biol 1992;37:945–52.
6. Tsukamoto Y, Fukutani S, Shin-Ike T, et al. Mineralized nodule formation by cultures of human dental pulp-derived fibroblasts. Arch Oral Biol 1992;37:1045–55.
7. Nakashima M, Nagasawa H, Yamada Y, Reddi AH. Regulatory role of transforming growth factor-beta, bone morphogenetic protein-2, and protein-4 on gene expression of extracellular matrix proteins and differentiation of dental pulp cells. Dev Biol 1994;162:18–28.
8. Shiba H, Fujita T, Doi N, et al. Differential effects of various growth factors and cytokines on the syntheses of DNA, type I collagen, laminin, fibronectin, osteonectin/secreted protein, acidic and rich in cysteine (SPARC), and alkaline phosphatase by human pulp cells in culture. J Cell Physiol 1998;174:194–205.
9. Buurma B, Gu K, Rutherford RB. Transplantation of human pulpal and gingival fibroblasts attached to synthetic scaffolds. Eur J Oral Sci 1999;107:282–9.
10. Buchaille R, Couble ML, Magloire H, Bleicher F. Expression of the small leucine-rich proteoglycan osteoadherin/osteomodulin in human dental pulp and developing rat teeth. Bone 2000;27:265–70.
11. Bikfalvi A, Klein S, Pintucci G, Rifkin DB. Biological roles of fibroblast growth factor-2. Endocr Rev 1997;18:26–45.
12. Nugent MA, Iozzo RV. Fibroblast growth factor-2. Int J Biochem Cell Biol 2000;32:115–20.
13. Roberts-Clark DJ, Smith AJ. Angiogenic growth factors in human dentine matrix. Arch Oral Biol 2000;45:1013–6.

14. Tran-Hung L, Laurent P, Camps J, About I. Quantification of angiogenic growth factors released by human dental cells after injury. Arch Oral Biol 2008;53:9–13.
15. Smith AJ. Pulpal responses to caries and dental repair. Caries Res 2002;36:223–32.
16. Tran-Hung L, Mathieu S, About I. Role of human pulp fibroblasts in angiogenesis. J Dent Res 2006;85:819–23.
17. McNeil PL, Muthukrishnan L, Warder E, D'Amore PA. Growth factors are released by mechanically wounded endothelial cells. J Cell Biol 1989;109:811–22.
18. Tanaka Y, Kimata K, Adams DH, Eto S. Modulation of cytokine function by heparan sulfate proteoglycans: sophisticated models for the regulation of cellular responses to cytokines. Proc Assoc Am Physicians 1998;110:118–25.
19. Takayama S, Murakami S, Shimabukuro Y, Kitamura M, Okada H. Periodontal regeneration by FGF-2 (bFGF) in primate models. J Dent Res 2001;80:2075–9.
20. Murakami S, Takayama S, Ikezawa K, et al. Regeneration of periodontal tissues by basic fibroblast growth factor. J Periodontal Res 1999;34:425–30.
21. Murakami S, Takayama S, Kitamura M, et al. Recombinant human basic fibroblast growth factor (bFGF) stimulates periodontal regeneration in class II furcation defects created in beagle dogs. J Periodontal Res 2003;38:97–103.
22. Hirano F, Hirano H, Hino E, et al. CD44 isoform expression in periodontal tissues: cell-type specific regulation of alternative splicing. J Periodontal Res 1997;32:634–45.
23. Yanagita M, Kashiwagi Y, Kobayashi R, Tomoeda M, Shimabukuro Y, Murakami S. Nicotine inhibits mineralization of human dental pulp cells. J Endod 2008;34: 1061–5.
24. Bessey OA, Lowry OH, Brock MJ. A method for the rapid determination of alkaline phosphatase with five cubic millimeters of serum. J Biol Chem 1946;164:321–9.
25. Labarca C, Paigen K. A simple, rapid, and sensitive DNA assay procedure. Anal Biochem 1980;102:344–52.
26. Dahl LK. A simple and sensitive histochemical method for calcium. Proc Soc Exp Biol Med 1952;80:474–9.
27. Smith JT, Tomfohr JK, Wells MC, Beebe TP Jr., Kepler TB, Reichert WM. Measurement of cell migration on surface-bound fibronectin gradients. Langmuir 2004;20: 8279–86.
28. Takayama S, Murakami S, Miki Y, et al. Effects of basic fibroblast growth factor on human periodontal ligament cells. J Periodontal Res 1997;32:667–75.
29. Spoto G, Fioroni M, Rubini C, Tripodi D, Di Stilio M, Piattelli A. Alkaline phosphatase activity in normal and inflamed dental pulps. J Endod 2001;27:180–2.
30. Okabe T, Sakamoto M, Takeuchi H, Matsushima K. Effects of pH on mineralization ability of human dental pulp cells. J Endod 2006;32:198–201.
31. Nakashima M, Mizunuma K, Murakami T, Akamine A. Induction of dental pulp stem cell differentiation into odontoblasts by electroporation-mediated gene delivery of growth/differentiation factor 11 (Gdf11). Gene Ther 2002;9:814–8.
32. Grando Mattuella L, Westphalen Bento L, de Figueiredo JA, Nor JE, de Araujo FB, Fossati AC. Vascular endothelial growth factor and its relationship with the dental pulp. J Endod 2007;33:524–30.
33. Smith AJ, Matthews JB, Hall RC. Transforming growth factor-beta1 (TGF-beta1) in dentine matrix: ligand activation and receptor expression. Eur J Oral Sci 1998; 106(Suppl 1):179–84.
34. Russo LG, Maharajan P, Maharajan V. Basic fibroblast growth factor (FGF-2) in mouse tooth morphogenesis. Growth Factors 1998;15:125–33.
35. Cam Y, Neumann MR, Oliver L, Raulais D, Janet T, Ruch JV. Immunolocalization of acidic and basic fibroblast growth factors during mouse odontogenesis. Int J Dev Biol 1992;36:381–9.
36. Martin A, Unda FJ, Begue-Kirn C, Ruch JV, Arechaga J. Effects of aFGF, bFGF, TGFbeta1 and IGF-I on odontoblast differentiation in vitro. Eur J Oral Sci 1998; 106(Suppl 1):117–21.
37. Nakashima M. The effects of growth factors on DNA synthesis, proteoglycan synthesis and alkaline phosphatase activity in bovine dental pulp cells. Arch Oral Biol 1992; 37:231–6.
38. Shiba H, Nakamura S, Shirakawa M, et al. Effects of basic fibroblast growth factor on proliferation, the expression of osteonectin (SPARC) and alkaline phosphatase, and calcification in cultures of human pulp cells. Dev Biol 1995;170:457–66.
39. Mullane EM, Dong Z, Sedgley CM, et al. Effects of VEGF and FGF2 on the revascularization of severed human dental pulps. J Dent Res 2008;87:1144–8.
40. Shimabukuro Y, Ueda M, Ichikawa T, et al. Fibroblast growth factor-2 stimulates hyaluronan production by human dental pulp cells. J Endod 2005;31: 805–8.
41. Comper WD, Laurent TC. Physiological function of connective tissue polysaccharides. Physiol Rev 1978;58:255–315.
42. Weigel PH, Frost SJ, McGary CT, LeBoeuf RD. The role of hyaluronic acid in inflammation and wound healing. Int J Tissue React 1988;10:355–65.
43. Oksala O, Salo T, Tammi R, et al. Expression of proteoglycans and hyaluronan during wound healing. J Histochem Cytochem 1995;43:125–35.
44. West DC, Hampson IN, Arnold F, Kumar S. Angiogenesis induced by degradation products of hyaluronic acid. Science 1985;228:1324–6.
45. Ruggiero SL, Bertolami CN, Bronson RE, Damiani PJ. Hyaluronidase activity of rabbit skin wound granulation tissue fibroblasts. J Dent Res 1987;66:1283–7.
46. Noble PW. Hyaluronan and its catabolic products in tissue injury and repair. Matrix Biol 2002;21:25–9.
47. Love SH, Shannon BT, Myrvik QN, Lynn WS. Characterization of macrophage agglutinating factor as a hyaluronic acid-protein complex. J Reticuloendothel Soc 1979; 25:269–82.
48. Kikuchi N, Kitamura C, Morotomi T, et al. Formation of dentin-like particles in dentin defects above exposed pulp by controlled release of fibroblast growth factor 2 from gelatin hydrogels. J Endod 2007;33:1198–202.
49. Goldberg M, Septier D, Rapoport O, et al. Targeted disruption of two small leucine-rich proteoglycans, biglycan and decorin, excerpts divergent effects on enamel and dentin formation. Calcif Tissue Int 2005;77:297–310.

Skeletal myoblast sheet transplantation improves the diastolic function of a pressure-overloaded right heart

Takaya Hoashi, MD,[a] Goro Matsumiya, MD, PhD,[a] Shigeru Miyagawa, MD, PhD,[a] Hajime Ichikawa, MD, PhD,[a] Takayoshi Ueno, MD, PhD,[a] Masamichi Ono, MD, PhD,[a] Atsuhiro Saito, PhD,[a] Tatsuya Shimizu, MD, PhD,[b] Teruo Okano, MD, PhD,[b] Naomasa Kawaguchi, PhD,[c] Nariaki Matsuura, MD, PhD,[c] and Yoshiki Sawa, MD, PhD[a]

Objective: The development of right ventricular dysfunction has become a common problem after surgical repair of complex congenital heart disease. A recent study reported that tissue-engineered skeletal myoblast sheet transplantation improves left ventricular function in patients with dilated and ischemic cardiomyopathy. Therefore myoblast sheet transplantation might also improve ventricular performance in a rat model of a pressure-overloaded right ventricle.

Methods: Seven-week-old male Lewis rats underwent pulmonary artery banding. Four weeks after pulmonary artery banding, myoblast sheet transplantation to the right ventricle was performed in the myoblast sheet transplantation group (n = 20), whereas a sham operation was performed in the sham group (n = 20).

Results: Four weeks after performing the procedure, a hemodynamic assessment with a pressure–volume loop showed a compensatory increase in systolic function in both groups. However, only the myoblast sheet transplantation group showed a significant improvement in the diastolic function: end-diastolic pressure (sham vs myoblast sheet transplantation, 10.3 ± 3.1 vs 5.0 ± 3.7 mm Hg; $P < .001$), time constant of isovolumic relaxation (11.1 ± 2.5 vs 7.6 ± 1.2 ms, $P < .001$), and end-diastolic pressure–volume relationship (16.1 ± 4.5 vs 7.6 ± 2.4/mL, $P < .005$). The right ventricular weight and cell size similarly increased in both groups. A histologic assessment demonstrated significantly suppressed ventricular fibrosis and increased capillary density in the myoblast sheet transplantation group in comparison with those in the sham group. Reverse transcription–polymerase chain reaction demonstrated an increased myocardial gene expression of hepatocyte growth factor and vascular endothelial growth factor in the myoblast sheet transplantation group but not in the sham group.

Conclusions: Skeletal myoblast sheet transplantation improved the diastolic dysfunction and suppressed ventricular fibrosis with increased capillary density in a rat model of a pressure-overloaded right ventricle. This method might become a novel strategy for the myocardial regeneration of right ventricular failure in patients with congenital heart disease.

Because of recent developments in diagnostic methods, the establishment of new surgical techniques, and improvements in perioperative management, patients with complex congenital heart disease (CHD) are today often able to survive to adulthood. However, even after a successful repair, right ventricular (RV) overload remains in some patients, in whom it impairs RV function and influences long-term mortality and morbidity.[1-3] Chronic pressure overload is one of the major risk factors of RV dysfunction. In this situation the right ventricle is hypertrophied and systolic function is initially preserved, whereas diastolic function gradually deteriorates.[4,5] Prolonged exposure to excessive pressure overload results in irreversible RV failure. Clinically, the relationship between progressive fibrosis and RV function must be addressed.[6-8]

Recently, cardiac regeneration therapy has provided a new treatment for end-stage heart failure, and skeletal myoblasts are currently thought to be a potential cell source.[9-11] We developed a novel cell delivery system using temperature-responsive culture dishes,[12] and tissue-engineered cell sheets have been created without any scaffold, which maintains cell–cell interaction and extracellular matrix while avoiding any inflammatory reaction, and with improved cell survival.[13] Skeletal myoblast sheet transplantation (MST) has been shown to improve left ventricular (LV) contractility in several animal models of LV failure.[14-16] Otherwise, it is unclear whether MST can also affect the right ventricle, especially pressure-induced RV dysfunction. Hence this study assessed whether MST could improve RV function in rats after damage caused by pressure overload.

From the Department of Cardiovascular Surgery,[a] Osaka University Graduate School of Medicine, Osaka, Japan; the Institute of Advanced Biomedical Engineering and Science,[b] Tokyo Women's Medical University, Tokyo, Japan; and the Department of Molecular Pathology,[c] Osaka University Graduate School of Allied Health Science, Osaka, Japan.

Received for publication March 17, 2008; revisions received Oct 1, 2008; accepted for publication Feb 2, 2009.

Address for reprints: Yoshiki Sawa, MD, PhD, 2–2 Yamadaoka, Suita, Osaka 565-0871, Japan (E-mail: sawa@surg1.med.osaka-u.ac.jp).

J Thorac Cardiovasc Surg 2009;138:460-7
0022-5223/$36.00

doi:10.1016/j.jtcvs.2009.02.018

Abbreviations and Acronyms

BW = body weight
CFR = coronary flow reserve
EDPVR = end-diastolic pressure–volume relationship
Ees = end-systolic elastance
ESPVR = end-systolic pressure–volume relationship
GAPDH = glyceraldehyde-3-phosphate dehydrogenase
HGF = hepatocyte growth factor
IVS = intraventricular septum
LV = left ventricular
MS = myoblast cell sheet
MST = myoblast sheet transplantation
PA = pulmonary artery
PAB = pulmonary artery banding
PRSW = preload recruitable stroke work
RT-PCR = reverse transcription–polymerase chain reaction
RV = right ventricular
SW = stroke work
VEGF = vascular endothelial growth factor

MATERIALS AND METHODS

Animal Care

All experimental procedures and protocols used in this investigation were reviewed and approved by the institutional animal care and use committee and are in accordance with the National Institutes of Health "Guide for the care and use of laboratory animals" (National Institutes of Health publication no. 85-23, revised 1996).

Creation of Chronic RV Pressure Overload

A rat model of pulmonary artery banding (PAB) was established to create chronic RV pressure overload. Seven-week-old male Lewis rats (180–210 g) were anesthetized with an intraperitoneal injection of ketamine hydrochloride (50 mg/kg) and xylazine (5 mg/kg) and ventilated by using a volume-controlled respirator (2 mL, 60 cycles/min) with room air. A left thoracotomy was performed at the fourth intracostal space, and the main pulmonary artery (PA) was carefully exposed. As previously reported,[17] a 19-gauge injection needle (outer diameter, 1.1 mm) was placed alongside the PA, and a 3-0 polyester suture was tied tightly around the PA and the needle. Next, the needle was rapidly removed, and then a fixed diameter was set for the PA. Thereafter, the thorax was closed in layers, and the ventilator setting was changed (90 cycles/min) for half an hour to reduce the respiratory load.

Skeletal Myoblast Sheet Preparation

Creation of myoblast cell sheets (MSs) with temperature-responsive culture dishes (UpCell; Cellseed, Tokyo, Japan) was done according to previous reports.[14-16] Briefly, skeletal muscle was harvested from the hind legs of 4-week-old syngeneic rats. The purified myoblasts were incubated on 35-mm UpCell dishes at 37°C, with the cell numbers adjusted to 3×10^6 per dish. After 12 to 18 hours, the dishes were moved to a refrigerator set at 20°C and left there for 30 minutes. During that time, the MSs detached spontaneously from the surfaces. Each sheet measured from 10 to 15 mm in diameter.

Skeletal MST

Four weeks after PAB, a second left thoracotomy was performed at the fifth intracostal space after achievement of general anesthesia. After opening the pericardium, the RV anterior wall was exposed. Two MSs were grafted onto each anterior wall of the right ventricle in the MST group (n = 20), or a sham operation was performed in the sham group (n = 20). The pericardium was closed linearly before the thorax was closed to prevent the dislocation of MSs. In addition, age-matched rats that did not undergo surgical intervention were also prepared as a control group (n = 20).

Hemodynamic Study and Data Analysis

Four weeks after the MST or sham operation, 10 rats in each group were anesthetized and ventilated again and were set on the blanket warmer to maintain body temperature. A median sternotomy was performed, and the pericardium was opened carefully to minimize hemorrhaging. A silk thread was placed under the inferior vena cava just above the diaphragm to change the RV preload. After purse-string sutures were attached with 7-0 polypropylene, the conductance catheter (Unique Medical Co, Tokyo, Japan) was inserted through the RV apex toward the pulmonary valve along the longitudinal axis of the RV cavity and then fixed. A Miller 1.4F pressure-tip catheter (SPR-719; Millar Instruments, Houston, Tex) was also inserted from the RV anterior wall and fixed. For better volume measurement, a 1-mm curve was added to the original standard straight conductance catheter to fit the complex RV geometry. The position of the conductance catheter was determined by observing the pressure and segmental volume signals with the appropriate phase relationships. The conductance system and the pressure transducer controller (Integral 3 [VPR-1002], Unique Medical Co) were set as previously reported.[18] Pressure–volume loops and intracardiac electrocardiograms were monitored online, and the conductance, pressure, and intracardiac electrocardiographic signals were analyzed with Integral 3 software (Unique Medical Co).[18]

Under stable hemodynamic conditions, the baseline indices were initially measured, and then the pressure–volume loop was drawn during inferior vena caval occlusion and analyzed (Figure 1). Finally, the conductivity of the sampled blood was measured with a small (0.1 mm) cuvette, and the parallel conductance volume was measured with the hypertonic saline dilution method to obtain the absolute volumes.[19]

The following indices were calculated as the baseline RV function: heart rate, end-systolic pressure, end-diastolic pressure, dP/dtmax, dP/dtmin, and the time constant of isovolumic relaxation (τ). The following relationships were determined by means of pressure–volume loop analysis as load-independent measures of RV function: end-systolic pressure–volume relationship (ESPVR), end-diastolic pressure–volume relationship (EDPVR), and preload recruitable stroke work (PRSW).

The ESPVR is linear, and it can be characterized by a slope (end-systolic elastance [Ees]) and a volume axis intercept (Vo), so that $Pes = Ees(Ves–Vo)$, where Pes and Ves are the end-systolic pressure and volume, respectively.[20]

In contrast, the EDPVR is intrinsically thought to be nonlinear. The relationship between the end-diastolic pressure (Ped) and volume (Ved) can be fitted to the monoexponential, so that $Ped = Po+be^{KvVed}$, where Po is the pressure asymptote (generally close to 0 mm Hg), b is a constant, and Kv is the variable represented as a ventricular stiffness property.[21]

The relationship between ventricular stroke work (SW) and end-diastolic volume (Ved) is represented as PRSW. PRSW is thought to be a suitable parameter of the contractile state and fitted to the following equation: $SW = K(Ved–Vo)$, where K is a constant as a potential measure of intrinsic myocardial performance independent of loading, geometry, and heart rate.[22]

Histopathologic Analysis

The other 10 rats in each group were killed 4 weeks after the sham or MST operation for histologic analysis, reverse transcription–polymerase chain reaction (RT-PCR), and blood sampling. The hearts were quickly removed, and the ventricles were dissected free of atrial tissue and large

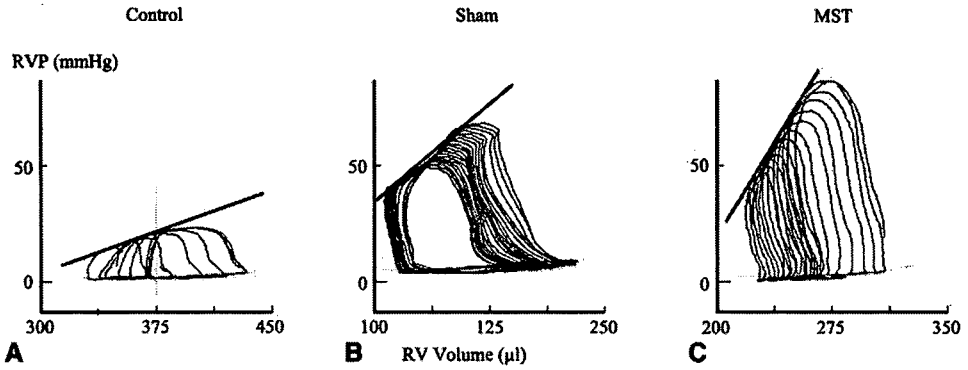

FIGURE 1. Representative pressure–volume loops of the control (A), sham (B), and myoblast sheet transplantation (*MST*; C) groups under different loading conditions. The slope of the end-systolic pressure–volume relationship is displayed as a *black straight line*. The correlation of the end-diastolic pressure–volume relationship is displayed as a *green monoexponential curve*. *RVP*, Right ventricular pressure; *RV*, right ventricle.

blood vessels. The right ventricle was carefully separated from the left ventricle and intraventricular septum (IVS). The fresh ventricular tissues were immediately blotted dry and weighted separately to determine the degree of RV hypertrophy based on 2 parameters: RV wall weight/body weight (RV/BW) and RV wall weight/LV and IVS wall weight (RV/LV+IVS).

Tissue specimens were obtained from the endocardium, the midwall, and the epicardium of the RV anterior wall in cross-sections, cut into 5-μm-thick sections, and stained with hematoxylin and eosin for morphologic analysis, including measurement of RV wall thickness, periodic acid–Schiff staining to measure the short-axis length of the RV myocardial cell, Factor VIII–related antigen staining (Dako EPOS anti-human Von Willebrand factor/HRP; Dako Cytomation, Glostrup, Denmark) to quantify capillary vascular density, and Masson trichrome staining for determination of the amount of interstitial and myocardial fibrosis. The percentage of interstitial and myocardial fibrosis were assessed by a computer-based method[23,24] with the use of a software filter (Mac Scope Software; MITANI Corp, Tokyo, Japan), which can recognize the distinct color shades. The number of pixels of the blue-stained collagen area was calculated, then divided by the total number of pixels in a field. Each 3 fields of the endocardial, epicardial, and mid layers of the RV wall per slide were analyzed and then averaged.

RT-PCR

Total RNA was isolated from the stored specimens by using the RNeasy Mini Kit (Qiagen, Hilden, Germany) and reverse transcribed with Omniscript Reverse Transcriptase (Qiagen). RT-PCR was performed with the ABI PRISM 7700 (Applied Biosystems, Foster City, Calif). Measurement of the mRNA expression of hepatocyte growth factor (HGF) and vascular endothelial growth factor (VEGF) was performed in triplicate. The results are expressed after normalization for glyceraldehyde-3-phosphate dehydrogenase (GAPDH).

Statistical Analysis

All data were expressed as the mean ± SEM and range. Student's unpaired *t* test or analysis of variance for parametric values was used to compare group means.

RESULTS

Pressure Overload and Hypertrophy of the Right Ventricle After PAB

After PAB, a weight analysis showed the heart weight/BW, RV/BW, and RV/(LV+IVS) weight ratios in the sham and MST groups to be similar and significantly higher than in the control group (Table 1). Both the sham and MST groups showed a significantly increased end-systolic pressure and dP/dtmax than seen in the control group (Table 2).

Hemodynamic Effects of MST

The baseline indices revealed that end-diastolic pressure and τ values were significantly increased only in the sham group in comparison with those in the control group but not in the MST group (Table 2). Typical examples of the pressure–volume loop in each group are presented in Figure 1. The pressure–volume loop analysis revealed that the ESPVR and PRSW values significantly increased both in the sham and MST groups. However, the EDPVR value significantly increased only in the sham group (control vs sham vs MST groups: 8.6 ± 2.9 vs 16.1 ± 4.5 vs 7.6 ± 2.4/mL; $P < .05$ in the control and MST groups vs the sham group; Table 2).

Histologic Effects of MST

Whole heart findings showed the RV wall thickened, the cavity enlarged, and the IVS shifted toward the left side in the sham and MST groups (Figure 2, *A*). In the MST group transplanted MSs were observed as an elastic thin layer on the epicardium (Figure 2, *B*). The RV wall thickness and myocardial cell size in the sham and MST groups were similar and significantly higher than in the control group (Figure 2, *C–E*).

TABLE 1. Weight analysis at the fourth week after the operation

Group	Control	Sham	MST
HW/BW (mg/g)	2.62 ± 0.09	3.53 ± 0.50*	4.03 ± 0.59*
RV/BW (mg/g)	0.54 ± 0.15	1.62 ± 0.42*	1.65 ± 0.32*
RV/(IVS+LV)	0.27 ± 0.08	0.69 ± 0.11*	0.69 ± 0.09*

MST, Myoblast sheet transplantation; *HW*, heart weight; *BW*, body weight; *RV*, right ventricle; *IVS*, interventricular septum; *LV*, left ventricle. *$P < .05$ versus the control group.

TABLE 2. Hemodynamic indices at the fourth week after the operation

Group	Control	Sham	MST
Basic hemodynamic indices			
HR (beats/min)	280 ± 72	233 ± 34	249 ± 65
ESP (mm Hg)	22.8 ± 2.9	82.3 ± 11.8*	78.7 ± 13.2*
EDP (mm Hg)	2.4 ± 1.4	10.3 ± 3.1*†	5.0 ± 3.7
dP/dtmax (mm Hg/s)	1301 ± 206	3197 ± 597*	3352 ± 1332*
dP/dtmin (mm Hg/s)	–997 ± 210	–2466 ± 582*	–2682 ± 828*
τ (ms)	7.9 ± 2.7	11.1 ± 2.5*†	7.6 ± 1.2
Load-independent parameters analyzed by PV loop			
ESPVR (mm Hg/mL)	538 ± 196	857 ± 305*	967 ± 201*
EDPVR (/mL)	8.6 ± 2.9	16.1 ± 4.5*†	7.6 ± 2.4
PRSW (mm Hg)	17.0 ± 4.1	40.2 ± 19.6*	40.8 ± 13.6*
PRSW/RV (mm Hg/kg)	88.3 ± 23.9	71.5 ± 31.3	73.6 ± 28.8

MST, Myoblast sheet transplantation; *HR*, heart rate; *ESP*, end-systolic pressure; *EDP*, end-diastolic pressure; *PV*, pressure–volume; *ESPVR*, end-systolic pressure–volume relationship; *EDPVR*, end-diastolic pressure–volume relationship; *PRSW*, preload-recruitable stroke work; *RV*, right ventricular weight. *$P < .05$ versus the control group. †$P < .05$ versus the MST group.

Factor VIII stain showed that myocardial capillary vascular density showed no significant difference at the mid layer and endocardial layer (Figure 3, *B* and *C*), but it was significantly higher in the MST group than in the other 2 groups at the epicardial layer (Figure 3, *A*). Hence, total capillary density in the MST group was significantly higher than in the other 2 groups (control vs sham vs MST groups: 262 ± 98 vs 271 ± 289 vs 823 ± 708; $P < 0.05$ in the control and sham groups vs the MST group; Figure 3, *D*).

Periodic acid–Schiff staining demonstrated significant interstitial fibrosis of the right ventricle in both the sham and MST groups, but the percentage of fibrosis in the

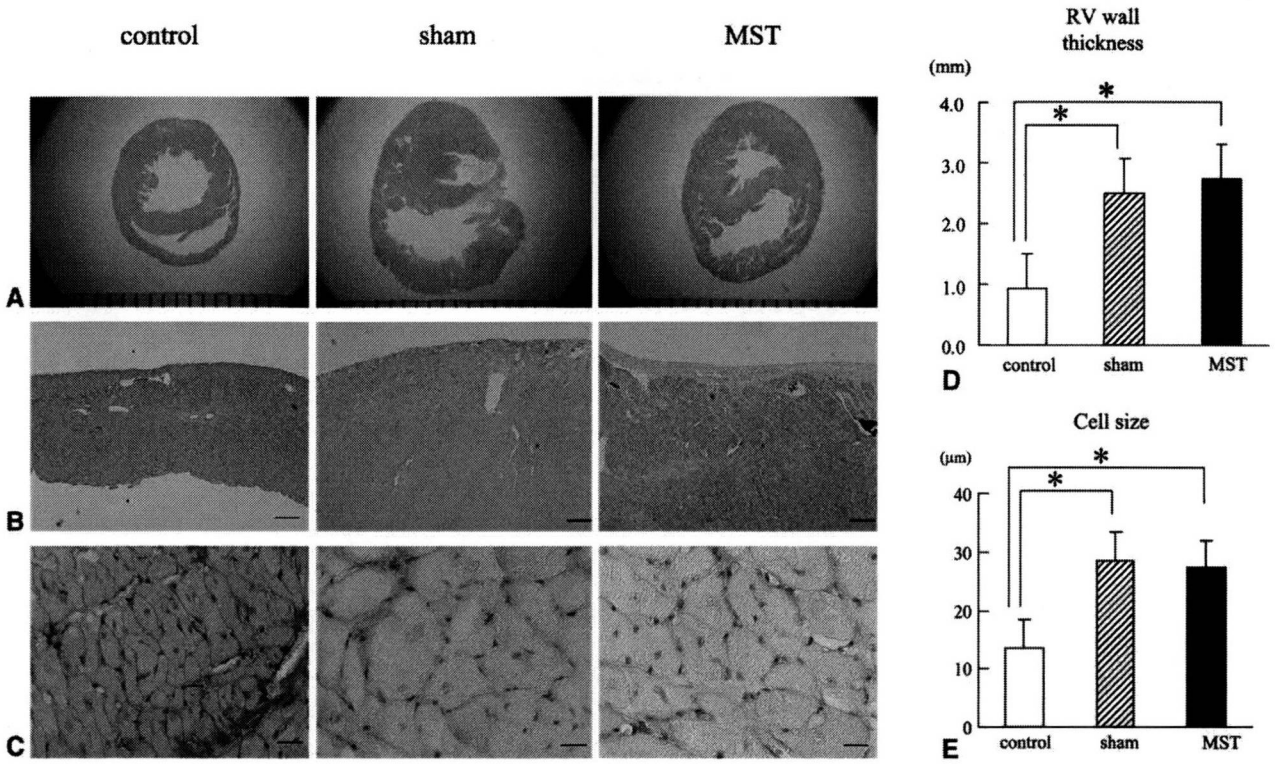

FIGURE 2. Macroscopic photographs of hematoxylin and eosin–stained sections showing right ventricular *(RV)* wall thickening, cavity enlarging, and the intraventricular septum shifting towered the left side in the sham and myoblast sheet transplantation *(MST)* groups (A and D). Photomicrographs (40×, scale bar = 200 μm) of hematoxylin and eosin–stained sections showed a fibrous organized thin layer on the epicardium in the myoblast sheet transplantation group (B). Photomicrographs (400×, scale bar = 20 μm) of periodic acid–Schiff–stained sections showed significantly hypertrophied ventricular myocytes in the sham and myoblast sheet transplantation groups (C and E). *$P < .05$ (n = 10).

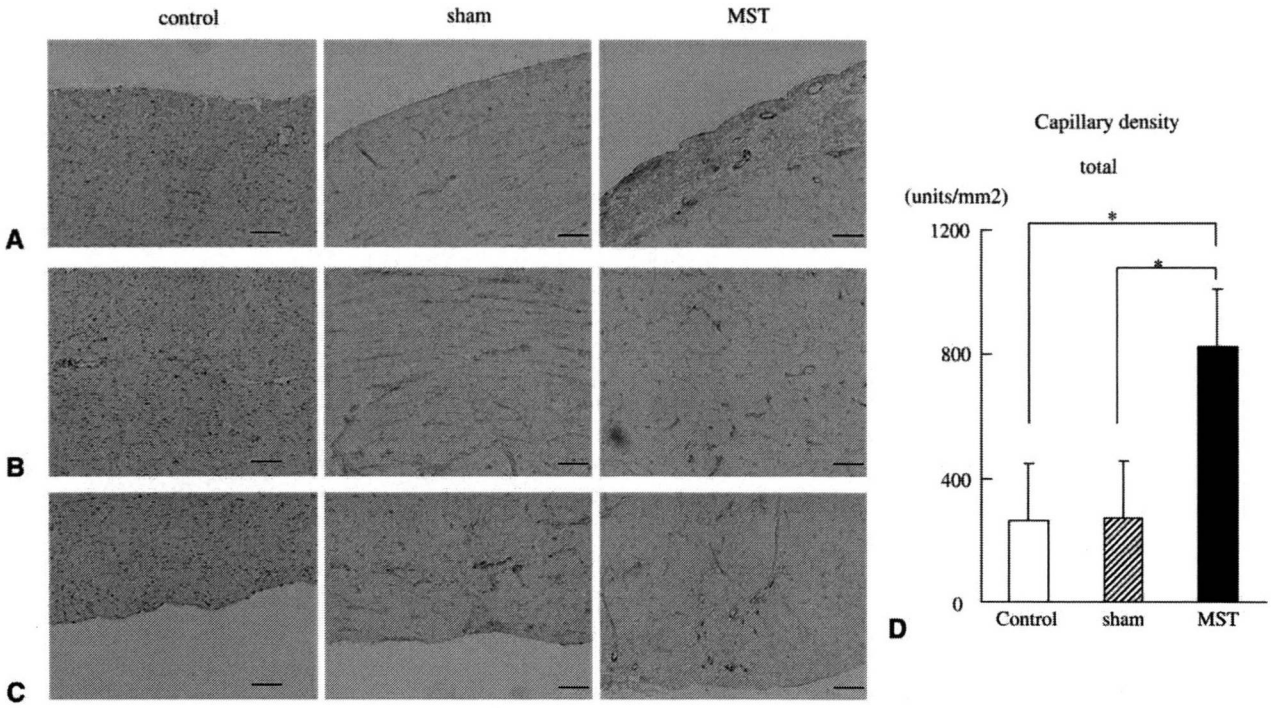

FIGURE 3. Representative photomicrographs (100×, scale bar = 100 μm) of Factor VIII–stained epicardial layer (A), mid layer (B), and endocardial layer (C). Neovascularization occurred at the epicardial layer in the myoblast sheet transplantation *(MST)* group (D). *$P < .05$ (n = 10).

MST group was significantly less than that in the sham group (control vs sham vs MST groups: 4.8% ± 1.1% vs 24.5% ± 10.0% vs 19.0% ± 5.1%; $P < .05$ between each 2 groups; Figure 4, *A* and *E*). Aggregated endomyocardial fibrosis was detected only in the sham group (endomyocardial percentage of fibrosis, control vs sham vs MST groups: 5.7% ± 0.1% vs 31.5% ± 8.4% vs 18.6% ± 5.9%; $P < .01$ in the control and MST groups vs the sham group; Figure 4, *B–D* and *F*).

RT-PCR

The expression of HGF and VEGF mRNA in the MST group was significantly higher than in the sham group (control vs sham vs MST groups: HGF, 0.00009 ± 0.00008 vs 0.00041 ± 0.00030 vs 0.00073 ± 0.00031/GAPDH [$P < .05$ in each group]; *VEGF*, 0.00242 ± 0.00164 vs 0.00329 ± 0.00181 vs 0.00512 ± 0.00113/GAPDH [$P < .05$ in the control and sham group vs the MST group]; Figure 5).

DISCUSSION

This study demonstrated that skeletal MST improved diastolic function in a pressure-overloaded right heart model in rats by means of PAB. This conclusion is supported by the following evidence: (1) the diastolic function was significantly improved based on hemodynamic assessment and pressure–volume loop analysis; (2) interstitial and endocardial fibrosis was ameliorated, and capillary vascular density of the epicardial layer was increased; and (3) myocardial gene expression of HGF and VEGF was significantly increased. MST has been shown to have therapeutic effects in several models of LV failure.[14-16] However, the present results are the first to show evidence that MST is effective for the treatment of RV dysfunction resulting from chronic pressure overload.

Prolonged RV pressure overload promotes unique morphologic, histologic, and functional changes. The mechanical stimulation of pressure overload extends the myocardium, which leads to diastolic dysfunction.[21] Simultaneously, hypertrophied myocardium upregulates the release of various chemical mediators,[17] which induce further myocardial expansion, apoptosis, necrosis, and fibrosis, finally resulting in RV decompensation. Otherwise, ventricular hypertrophy itself reduces the coronary flow reserve (CFR) and leads to coronary microcirculatory dysfunction.[25] As studies on the left ventricle show, this phenomenon is detected particularly in the subendocardium.[26] The shortage of CFR induces myocardial cellar mortality and endocardial fibrosis, which accelerates ventricular dysfunction. The present and previous data indicate that transplanted elastic cells initially improved ventricular stiffness[14] and preserved CFR in the hypertrophied myocardium, both of which generate a synergistic effect of the suppression of myocardial cell death and fibrosis, especially at the endocardial layer. Although an angiogenetic effect was observed with the increased myocardial gene expression of HGF and VEGF, we speculate this does not increase endocardial coronary flow directly because increased

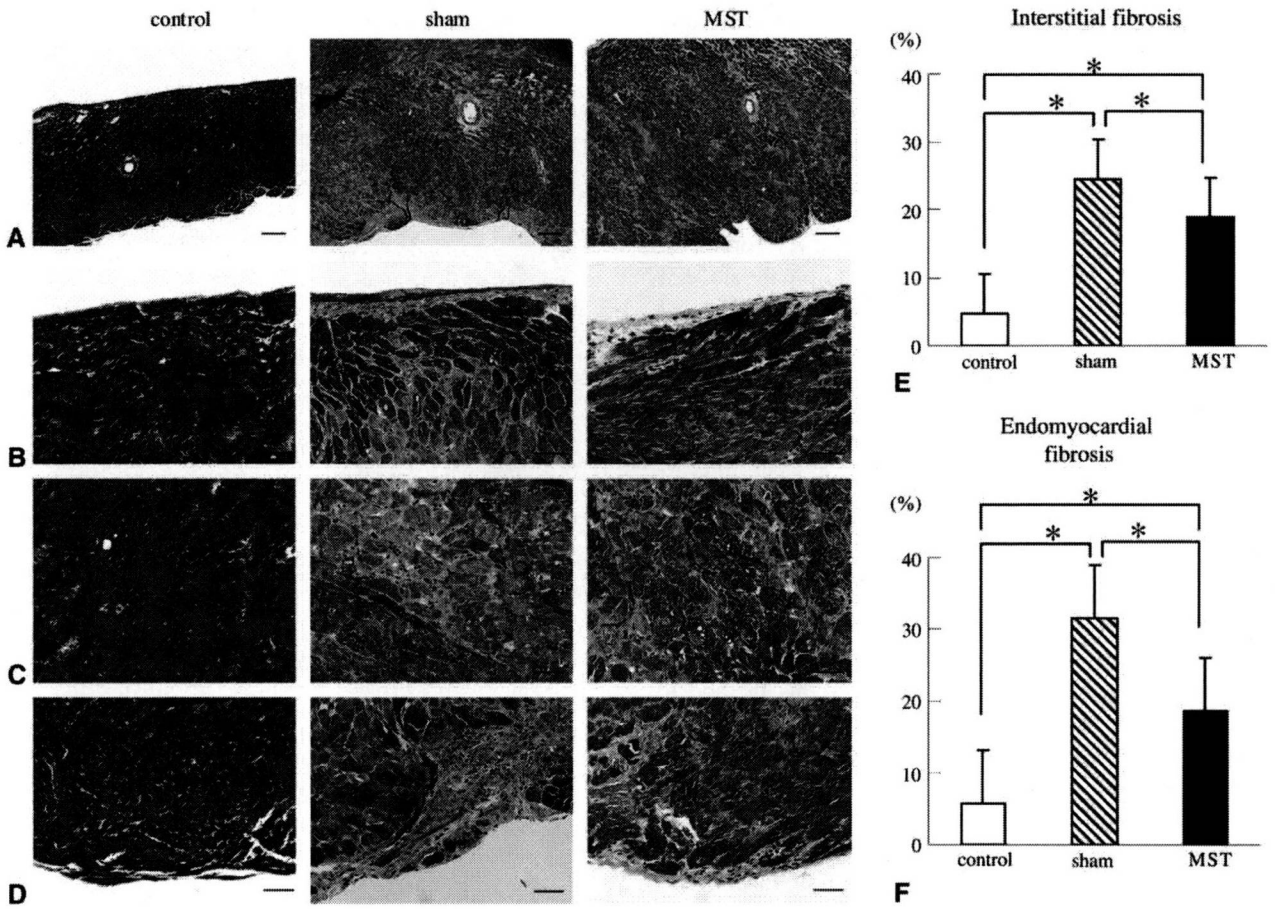

FIGURE 4. Representative photomicrographs of Masson's trichrome–stained transmural layer (A; 40×, scale bar = 200 μm), epicardial layer (B), mid layer (C), and endocardial layer (D; 200×, scale bar = 50 μm) for evaluation of interstitial (E) and endomyocardial (F) fibrosis. *$P < .05$ (n = 10).

capillary density was only seen at epicardial layer. These new capillaries might increase the blood supply to the transplanted myoblasts and prolong their survival.[13]

As several LV studies have previously shown, Lamberts and colleagues[27] revealed the strict relationship between RV chamber stiffness and the degree of myocardial fibrosis. In their report they also described that prevention or reduction of RV fibrosis improved RV diastolic dysfunction. Although we could not show any individual correlation between collagen contents and hemodynamic parameters in regard to diastolic function, these findings strongly support our results. Therefore we would like to emphasize that the suppression of fibrosis improved the RV diastolic function.

The hemodynamic assessment of cardiac performance of a hypertrophied right ventricle has not been established. Various attempts have been made; however, it is still necessary to perform cardiac catheterization to evaluate hemodynamics, especially regarding diastolic function.[28,29] Leeuwenburgh and associates[4] showed that RV compliance deteriorated in a lamb model and described τ and EDPVR values to be useful indicators for diastolic function. Gaynor

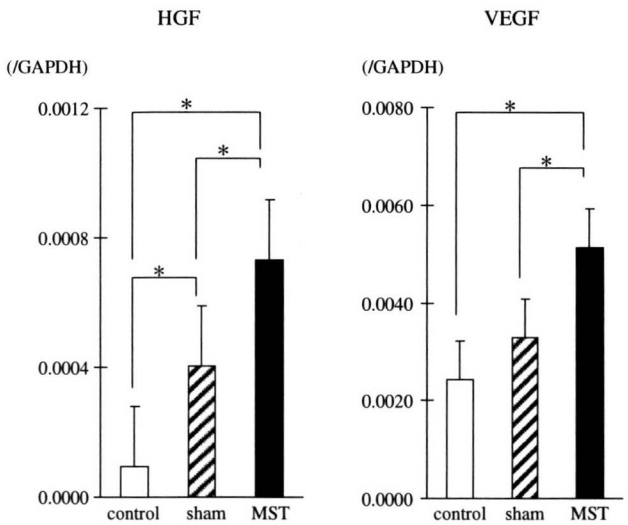

FIGURE 5. RT-PCR for evaluation of neurohormonal factor gene expression. The results are expressed after normalization for GAPDH. *HGF*, Hepatocyte growth factor; *VEGF*, vascular endothelial growth factor. *$P < .05$ (n = 10).

and coworkers[5] also showed an increase of EDPVR in a dog model of PAB. The current results are consistent with these reports. Therefore these data appear to be reliable.

On the other hand, the assessment of systolic function still remains controversial. In this study we showed that ESPVR (Ees) and PRSW were significantly increased in sham groups, as previously reported.[30] However, Dell'Italia and Walsh[31] pointed out that in the assessment of RV contractility, the slope of ESPVR (Ees) was different from the slope of the maximum time-varying elastance, which better reflected the RV contractility than Ees. In addition to Ees, PRSW is thought to be an optimal parameter of ventricular contractility. However, we might have to consider the discrepancy of the cardiac mass between normal and hypertrophied hearts because ventricular SW should be assessed as a per-unit cardiac mass. We tried to calculate the PRSW divided for each animal's RV weight, which revealed there was no statistical significance among the 3 groups (control vs sham vs MST groups: 88.3 ± 23.9 vs 71.5 ± 31.3 vs 73.6 ± 28.8 mm Hg/kg, Table 2). Hence it is hard to say that the RV pressure load induced a further improvement in RV contractility.

We need further investigation to apply this method to clinical RV failure because we did not ascertain the effect of MST on RV systolic function. Nevertheless, enormous fibrosis was seen in the sham group, and systolic function was still compensated until the timing of hemodynamic evaluation. However, previous reports showed that MST had an excellent effect on LV contractility.[14-16] Therefore we expect that this method might become a novel and potentially effective treatment strategy for patients with RV failure.

In conclusion, chronic pressure overload to the right ventricle caused hypertrophy and impaired diastolic function in rats. Skeletal MST attenuated diastolic dysfunction, which was mainly caused by suppressed interstitial and endocardial fibrosis. This method might become a novel strategy for the myocardial regeneration of RV failure in patients with CHD in the future.

We thank Mrs Masako Yokoyama for her expert assistance with RT-PCR and Kazuhiro Takekita and Takeshi Miki for technical support in creating the tissue-engineered skeletal MSs.

References

1. Bolger AP, Coats AJ, Gatzoulis MA. Congenital heart disease: the original heart failure syndrome. *Eur Heart J*. 2003;24:970-6.
2. Murphy JG, Gersh BJ, Mair DD, Fuster V, McGoon MD, Ilstrup DM, et al. Long-term outcome in patients undergoing surgical repair of tetralogy of Fallot. *N Engl J Med*. 1993;329:593-9.
3. Gatzoulis MA, Balaji S, Webber SA, Siu SC, Hokanson JS, Poile C, et al. Risk factors for arrhythmia and sudden cardiac death late after repair of tetralogy of Fallot: a multicentre study. *Lancet*. 2000;356:975-81.
4. Leeuwenburgh BP, Steendijk P, Helbing WA, Baan J. Indexes of diastolic RV function: load dependence and changes after chronic RV pressure overload in lambs. *Am J Physiol Heart Circ Physiol*. 2002;282:1350-8.
5. Gaynor SL, Maniar HS, Bloch JB, Steendijk P, Moon MR. Right atrial and ventricular adaptation to chronic right ventricular pressure overload. *Circulation*. 2005;112:212-8.
6. Deanfield JE, Ho SY, Anderson RH, McKenna WJ, Allwork SP, Hallidie-Smith KA. Late sudden death after repair of tetralogy of Fallot: a clinicopathologic study. *Circulation*. 1983;67:626-31.
7. Babu-Narayan SV, Kilner PJ, Li W, Moon JC, Goktekin O, Davlouros PA, et al. Ventricular fibrosis suggested by cardiovascular magnetic resonance in adults with repaired tetralogy of Fallot and its relationship to adverse markers of clinical outcome. *Circulation*. 2006;113:405-13.
8. Chowdhury UK, Sathia S, Ray R, Singh R, Pradeep KK, Venugopal P. Histopathology of the right ventricular outflow tract and its relationship to clinical outcomes and arrhythmias in patients with tetralogy of Fallot. *J Thorac Cardiovasc Surg*. 2006;132:270-7.
9. Taylor DA, Atkins BZ, Hungspreugs P, Jones TR, Reedy MC, Hutcheson KA, et al. Regenerating functional myocardium: improved performance after skeletal myoblast transplantation. *Nat Med*. 1998;4:929-33.
10. Menasche P, Hagege AA, Scorsin M, Pouzet B, Desnos M, Duboc D, et al. Myoblast transplantation for heart failure. *Lancet*. 2001;357:279-80.
11. Hagege AA, Marolleau JP, Vilquin JT, Alheritiere A, Peyrard S, Duboc D, et al. Skeletal myoblast transplantation in ischemic heart failure: long-term follow-up of the first phase I cohort of patients. *Circulation*. 2006;114:108-13.
12. Okano T, Yamada N, Sakai H, Sakurai Y. A novel recovery system for cultured cells using plasma-treated polystyrene dishes grafted with poly(N-isopropylacrylamide). *J Biomed Mater Res*. 1993;27:1243-51.
13. Miyagawa S, Sawa Y, Sakakida S, Taketani S, Kondoh H, Memon IA, et al. Tissue cardiomyoplasty using bioengineered contractile cardiomyocyte sheets to repair damaged myocardium: their integration with recipient myocardium. *Transplantation*. 2005;80:1586-95.
14. Memon IA, Sawa Y, Fukushima N, Matsumiya G, Miyagawa S, Taketani S, et al. Repair of impaired myocardium by means of implantation of engineered autologous myoblast sheets. *J Thorac Cardiovasc Surg*. 2005;130:1333-41.
15. Kondoh H, Sawa Y, Miyagawa S, Sakakida-Kitagawa S, Memon IA, Kawaguchi N, et al. Longer preservation of cardiac performance by sheet-shaped myoblast implantation in dilated cardiomyopathic hamsters. *Cardiovasc Res*. 2006;69:466-75.
16. Hata H, Matsumiya G, Miyagawa S, Kondoh H, Kawaguchi N, Matsuura N, et al. Grafted skeletal myoblast sheets attenuate myocardial remodeling in pacing-induced canine heart failure model. *J Thorac Cardiovasc Surg*. 2006;132:918-24.
17. Lekanne Deprez RH, van den Hoff MJ, de Boer PA, Ruijter PM, Maas AA, Chamuleau RA, et al. Changing patterns of gene expression in the pulmonary trunk-banded rat heart. *J Mol Cell Cardiol*. 1998;30:1877-88.
18. Sato T, Shishido T, Kawada T, Miyano H, Miyashita H, Inagaki M, et al. ESPVR of in situ rat left ventricle shows contractility-dependent curvilinearity. *Am J Physiol Heart Circ Physiol*. 1998;274:H1429-34.
19. Baan J, van der Velde ET, de Bruin HG, Smeenk GJ, Koops J, van Dijk AD, et al. Continuous measurement of left ventricular volume in animals and humans by conductance catheter. *Circulation*. 1984;70:812-23.
20. Suga H, Sagawa K. Instantaneous pressure-volume relationships and their ratio in the excised, supported canine left ventricle. *Circ Res*. 1974;35:117-26.
21. Gaasch WH, Cole JS, Quinones MA, Alexander JK. Dynamic determinants of left ventricular diastolic pressure-volume relations in man. *Circulation*. 1975;51:317-23.
22. Glower DD, Spratt JA, Snow ND, Kabas JS, Davis JW, Olsen CO, et al. Linearity of the Frank-Starling relationship in the intact heart: the concept of preload recruitable stroke work. *Circulation*. 1985;71:994-1009.
23. Hoyt RH, Collins SM, Skorton DJ, Ericksen EE, Conyers D. Assessment of fibrosis in infarcted human hearts by analysis of ultrasonic backscatter. *Circulation*. 1985;71:740-4.
24. Vasiljević JD, Popović ZB, Otasević P, Popović ZV, Vidaković R, Mirić M, et al. Myocardial fibrosis assessment by semiquantitative, point-counting and computer-based methods in patients with heart muscle disease: a comparative study. *Histopathology*. 2001;38:338-43.
25. Murray PA, Vatner SF. Reduction of maximal coronary vasodilator capacity in conscious dogs with severe right ventricular hypertrophy. *Circ Res*. 1981;48:25-33.
26. Rajappan K, Rimoldi OE, Dutka DP, Ariff B, Pennell DJ, Sheridan DJ, et al. Mechanisms of coronary microcirculatory dysfunction in patients with aortic stenosis and angiographically normal coronary arteries. *Circulation*. 2002;105:470-6.
27. Lamberts RR, Caldenhoven E, Lansink M, Witte G, Vaessen RJ, St Cyr JA, et al. Preservation of diastolic function in monocrotaline-induced right ventricular hypertrophy in rats. *Am J Physiol Heart Circ Physiol*. 2007;293:H1869-76.

28. Haddad F, Hunt SA, Rosenthal DN, Murphy DJ. Right ventricular function in cardiovascular disease, part I: anatomy, physiology, aging, and functional assessment of the right ventricle. *Circulation.* 2008;117:1436-48.
29. Burkhoff D, Mirsky I, Suga H. Assessment of systolic and diastolic ventricular properties via pressure-volume analysis: a guide for clinical, translational, and basic researchers. *Am J Physiol Heart Circ Physiol.* 2005;289:H501-12.
30. Faber MJ, Dalinghaus M, Lankhuizen IM, Steendijk P, Hop WC, Schoemaker RG, et al. Right and left ventricular function after chronic pulmonary artery banding in rats assessed with biventricular pressure-volume loops. *Am J Physiol Heart Circ Physiol.* 2006;291:H1580-6.
31. Dell'Italia LJ, Walsh RA. Application of a time varying elastance model to right ventricular performance in man. *Cardiovasc Res.* 1988;22:864-74.

TEN-2009-0386-Komoda_1P
Type: research-article

TISSUE ENGINEERING: Part A
Volume 00, Number 00, 2009

DOI: 10.1089/ten.tea.2009.0386

Original Article

Reduction of *N*-Glycolylneuraminic Acid Xenoantigen on Human Adipose Tissue-Derived Stromal Cells/ Mesenchymal Stem Cells Leads to Safer and More Useful Cell Sources for Various Stem Cell Therapies

AU1 ▶

Hiroshi Komoda, M.D., Ph.D.,[1,2,*] Hanayuki Okura, M.S.,[1,3,4,*] Chun Man Lee, M.D., Ph.D.,[1,5] Nagako Sougawa, D.M.D., Ph.D.,[1] Tomoaki Iwayama, D.M.D.,[6] Tomoko Hashikawa, D.M.D., Ph.D.,[6] Ayami Saga, M.S.,[1] Aya Yamamoto-Kakuta, B.S.,[1] Akihiro Ichinose, M.D., Ph.D.,[7] Shinya Murakami, D.M.D., Ph.D.,[6] Yoshiki Sawa, M.D., Ph.D.,[3,5] and Akifumi Matsuyama, M.D., Ph.D.[1]

Adipose tissue is an attractive source for somatic stem cell therapy. Currently, human adipose tissue-derived stromal cells/mesenchymal stem cells (hADSCs/MSCs) are cultured with fetal bovine serum (FBS). Recently, however, not only human embryonic stem cell lines cultured on mouse feeder cells but also bone marrow-derived human MSCs cultured with FBS were reported to express *N*-glycolylneuraminic acid (Neu5Gc) xenoantigen. Human serum contains high titers of natural preformed antibodies against Neu5Gc. We studied the presence of Neu5Gc on hADSCs/MSCs cultured with FBS and human immune response mediated by Neu5Gc. Our data indicated that hADSCs/MSCs cultured with FBS expressed Neu5Gc and that human natural preformed antibodies could bind to hADSCs/MSCs. However, hADSCs/MSCs express complement regulatory proteins such as CD46, CD55, and CD59 and are largely resistant to complement-mediated cytotoxicity. hADSCs/MSCs cultured with FBS could be injured by antibody-dependent cell-mediated cytotoxicity mechanism. Further, human monocyte-derived macrophages could phagocytose hADSCs/MSCs cultured with FBS and this phagocytic activity was increased in the presence of human serum. Culturing hADSCs/MSCs with heat-inactivated human serum for a week could markedly reduce Neu5Gc on hADSCs/MSCs and prevent immune responses mediated by Neu5Gc, such as binding of human natural preformed antibodies, antibody-dependent cell-mediated cytotoxicity, and phagocytosis. Adipogenic and osteogenic differentiation potentials of hADSCs/MSCs cultured with heat-inactivated human serum were not less than that of those cultured with FBS. For stem cell therapies based on hADSCs/MSCs, hADSCs/MSCs that presented Neu5Gc on their cell surfaces after exposure to FBS should be cleaned up to be rescued from xenogeneic rejection.

Introduction

Adipose tissue is an attractive source for somatic cell therapy, because it is safe and abundant and many investigators have reported that the stromal cells derived from adipose tissue (adipose tissue-derived stromal cells [ADSCs]) could differentiate into various cell types.[1–4] ADSCs are also referred to as adipose tissue-derived mesenchymal stem cells (MSCs). Human ADSCs (hADSCs)/MSCs are very similar to bone marrow (BM)-derived human MSCs (hMSCs) and therefore reveal differentiation potential similar to BM-derived hMSCs.[5–7]

For stem cell therapies based on hMSCs including hADSCs/MSCs, it is essential that stem cells are handled and cultured in a manner that guarantees the efficacy and safety of the cellular therapy product. One such aspect is the choice

[1]Department of Somatic Stem Cell Therapy, Foundation for Biomedical Research and Innovation, Kobe, Hyogo, Japan.
[2]Department of Internal Medicine, National Hospital Organization Chiba Medical Center, Chiba, Japan.
[3]Department of Surgery, Osaka University Graduate School of Medicine, Suita, Osaka, Japan.
[4]Japan Society for the Promotion of Science, Tokyo, Japan.
[5]Medical Center for Translational Research, Osaka University Hospital, Suita, Osaka, Japan.
[6]Department of Periodontology, Division of Oral Biology and Disease Control, Osaka University Graduate School of Dentistry, Osaka, Japan.
[7]Department of Plastic Surgery, Kobe University Hospital, Kobe, Hyogo, Japan.
*These authors contributed equally to this work.

of cell culture medium and supplements. In principle, most investigators agree that all animal materials should be avoided to maximize product safety. Currently, however, hADSCs/MSCs are cultured with fetal bovine serum (FBS), and the clinical efficacy of BM-derived hMSCs in human disease has been investigated using hMSCs cultured with FBS in a number of clinical trials.[8–12]

Recently, not only human embryonic stem cell (hESC) lines cultured on mouse feeder cells but also BM-derived hMSCs cultured with FBS were reported to express *N*-glycolylneuraminic acid (Neu5Gc) xenoantigen,[13,14] the so-called Hanganutziu–Deicher antigen.[15] Humans are incapable of synthesizing the common mammalian sialic acid, Neu5Gc, because of an *Alu* transposon-mediated inactivation of the CMP-*N*-acetylneuraminic acid hydroxylase gene.[16,17] Despite this, both hESC lines and BM-derived hMSCs were reported to express the Neu5Gc, apparently originating from the mouse feeder layers, animal-derived components, and FBS.[13,14] The significant levels of Neu5Gc found on the surface of hESCs and hMSCs evidently originate from a Trojan Horse pathway involving endocytosis of extracellular glycoconjugates, delivery to the lysosome, release of Neu5Gc by lysosomal sialidase, active transport to the cytoplasm through the lysosomal sialic acid transporter, activation by CMP, and addition to nascent glycoproteins and glycolipids in the secretory pathway.[18] It is also possible that amphipathic molecules carrying Neu5Gc might be directly transferred into the hESC and hMSC plasma membranes.[19] Human serum contains high titers of natural preformed antibodies against Neu5Gc xenoantigen.[20–22] Thus, binding of these natural preformed antibodies may lead to immune responses such as complement-mediated cytotoxicity (CMC), antibody-dependent cell-mediated cytotoxicity (ADCC), and antibody-dependent cellular phagocytosis. However, these immune responses mediated by natural preformed antibodies against human stem cells remain in controversary.[13,23] This study was therefore undertaken to study the presence of Neu5Gc on hADSCs/MSCs cultured with FBS and the human immune responses mediated by Neu5Gc on hADSCs/MSCs.

Materials and Methods

Cells

hADSCs/MSCs were prepared as described previously[1,2] with modifications.[3,4] Adipose tissue was resected during plastic surgery in five human subjects (four men and one woman; age, 20–60 years) as excess discards. Ten to 50 g of subcutaneous adipose tissue was collected from each subject. All subjects provided informed consent. The protocol was approved by the Review Board for Human Research of the Kobe University Graduate School of Medicine, Osaka University Graduate School of Medicine and Foundation for Biomedical Research and Innovation. All subjects fasted for at least 10 h before surgery and none was being treated with steroids. The resected excess adipose tissue was minced and then digested in Hank's balanced salt solution (Gibco Invitrogen, Grand Island, NY) containing 0.075% collagenase type II (Sigma Aldrich, St. Louis, MO) at 37°C for 1 h. Digests were filtered with a cell strainer (BD Bioscience, San Jose, CA) and centrifuged at 800 *g* for 10 min. Erythrocytes were excluded using density gradient centrifugation with Lymphoprep ($d = 1.077$; Nycomed, Oslo, Norway). The cells were then plated using Dulbecco's modified Eagle's medium (DMEM; Gibco Invitrogen) with 10% defined FBS (Hyclone) and incubated for 24 h at 37°C. Following incubation, the adherent cells were washed extensively and treated with 0.2 g/L ethylenediaminetetraacetate (EDTA) solution (Nacalai Tesque, Kyoto, Japan), and the resulting suspended cells were replated at a density of 10,000 cells/cm^2 on human fibronectin-coated dishes (BD BioCoat) in a medium containing 60% DMEM-low glucose, 40% MCDB-201 medium (Sigma Aldrich), 1×insulin–transferrin–selenium (Gibco Invitrogen), 1 nM dexamethasone (Sigma Aldrich), 100 μM ascorbic acid 2-phosphate (Sigma Aldrich), 10 ng/mL epidermal growth factor (PeproTec, Rocky Hill, NJ), and 5% FBS. For analysis of the effects of human serum on Neu5Gc expression on hADSCs/MSCs, the cells were cultured for 7 days, where FBS was replaced by 5% heat-inactivated normal human pooled serum (NHS) from type AB blood. As control cells, a murine pancreatic cell line, Panc02, was cultured with RPMI 1640 medium (Gibco Invitrogen) supplemented with 10% FBS and 1% antibiotic/antimycotic solution.

Flow cytometry

Cells were detached from culture dishes and suspended in Dulbecco's phosphate-buffered saline (D-PBS; Nacalai Tesque). Aliquots (5×10^5 cells) were incubated for 30 min at 4°C with a chicken anti-Neu5Gc polyclonal antibody (a gift from Prof. N. Wakamiya, Asahikawa Medical College, Hokkaido, Japan).[24] Cells incubated with D-PBS alone were used as negative control. After washing with D-PBS, cells were stained with fluorescein isothiocyanate (FITC)-conjugated rabbit anti-chicken immunoglobulin G (IgG; Cappel) as a second antibody. After staining, the cells were washed and resuspended

FIG. 1. Expression of Neu5Gc on hADSCs/MSCs. (**A**) Specificity of anti-Neu5GC antibody. Panc02, a cell line derived from murine pancreatic carcinomas, expressed Neu5Gc. Flow cytometric analysis showed that chicken anti-Neu5Gc polyclonal antibody bound to the surfaces of Panc02, but Neu5Gc-preadsorbed anti-Neu5Gc polyclonal antibody could not react, showing specificity of the anti-Neu5Gc antibody. The percentage of cells that stained positive is indicated in the upper right corner of each panel. (**B**) Expression of Neu5Gc xenoantigen on hADSCs/MSCs. Fresh hADSCs/MSCs did not express Neu5Gc on their cell surface. In accordance with passage numbers, the population of Neu5Gc-positive cells increased by cultivation with FBS. The percentage of cells that stained positive is indicated in the upper right corner of each panel. (**C**) Reduction of Neu5Gc xenoantigen by chasing cultivation with human serum. After cultivation of hADSCs/MSCs with heat-inactivated NHS but not FBS, the percentages of Neu5Gc-positive cells have decreased in accordance with culture duration. The decrement manners of second passaged hADSCs/MSCs and fifth passaged ones have been in a similar fashion. The percentage of cells that stained positive is indicated in the upper right corner of each panel. Data are representative of four independent experiments. Neu5Gc, *N*-glycolylneuraminic acid; hADSCs/MSCs, human adipose tissue-stromal cells/mesenchymal stem cells; FBS, fetal bovine serum; NHS, normal human pooled serum; IgG, immunoglobulin G; M1; FL1.

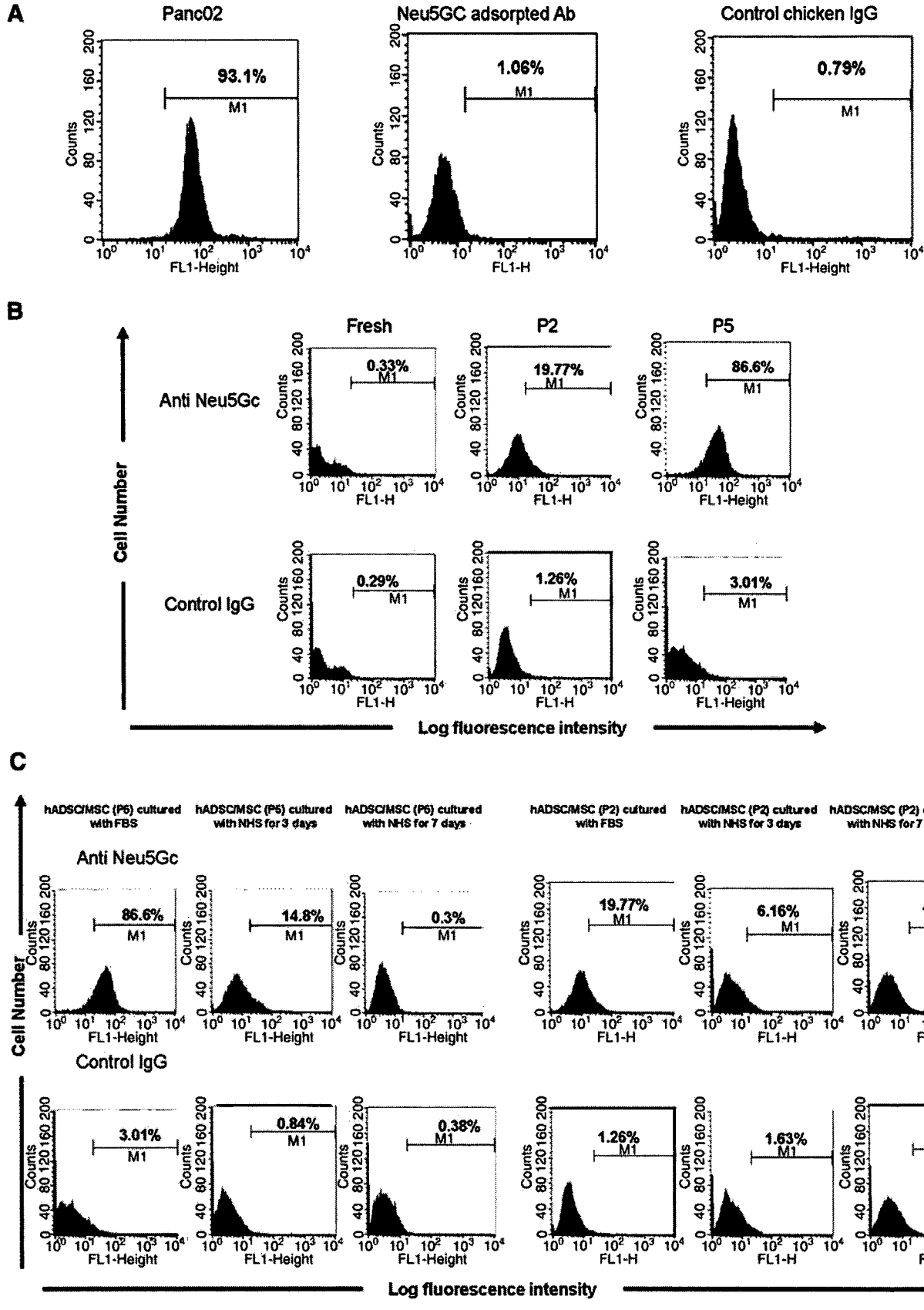
A
Panc02
93.1%
M1
Neu5GC adsorpted Ab
1.06%
M1
Control chicken IgG
0.79%
M1
Counts
FL1-Height
FL1-H
B
Fresh
P2
P5
Anti Neu5Gc
0.33%
19.77%
86.6%
Control IgG
0.29%
1.26%
3.01%
Cell Number
Log fluorescence intensity
C
hADSC/MSC (P6) cultured with FBS
hADSC/MSC (P6) cultured with NHS for 3 days
hADSC/MSC (P6) cultured with NHS for 7 days
hADSC/MSC (P2) cultured with FBS
hADSC/MSC (P2) cultured with NHS for 3 days
hADSC/MSC (P2) cultured with NHS for 7 days
Anti Neu5Gc
86.6%
14.8%
0.3%
19.77%
6.16%
1.83%
Control IgG
3.01%
0.84%
0.38%
1.26%
1.63%
1.73%
Cell Number
Log fluorescence intensity

U5 ▶ AU3 ▶ in D-PBS with 150 ng/mL 7-AAD (BD Pharmingen) to eliminate dead cells. The cells were analyzed by flow cytometry using a FACSCalibur flow cytometer and CellQuest Pro software (BD Biosciences). Data shown in figures are gated for live cells by excluding cells that stained positive for 7-AAD. Percentage of positive cells was defined against a 99% negative control exclusion gate. For detection of binding of human natural preformed antibodies, the cells were exposed to 10% fresh NHS or 5 mM Neu5Gc-preadsorbed NHS in D-PBS containing 15 mM EDTA for 30 min at 4°C. After washing, the cells were stained with FITC-conjugated goat anti-human IgG or IgM antibody (Cappel), or control goat IgG, respectively. To examine the blocking effects of anti-Neu5Gc antibody onto the surface of hADSCs/MSCs, hADSCs/MSCs cultured with FBS were precoated with anti-Neu5Gc antibody, exposed to 10% fresh NHS containing 15 mM EDTA, and then applied for flow cytometric analysis. Stained cells were washed and resuspended in D-PBS with 7-AAD and analyzed by a FACSCalibur flow cytometer. For detection of human complement regulatory proteins, cells were stained with FITC-conjugated mouse monoclonal antibodies to human CD46 (membrane cofactor protein), CD55 (decay accelerating factor), CD59, or control IgG (all from BD Pharmingen) and analyzed by a FACSCalibur flow cytometer as well.

Detection of complement deposition

The amounts of C4 and C3 fragments deposited on the cell surface were also analyzed by flow cytometry. The cells were detached by 0.25% trypsin/EDTA and subsequently incubated with 10% fresh NHS in DMEM for 30 min at 37°C. Cells incubated with DMEM alone or 10% fresh NHS in DMEM containing 15 mM EDTA was used as negative control. After washing with cold D-PBS three times, the cells were stained with FITC-conjugated rabbit anti-human C4c or AU3 ▶ C3c antibody (Dako). After staining, the cells were washed and resuspended in 500 μL of D-PBS with 7-AAD and analyzed by a FACSCalibur flow cytometer.

CMC assay

CMC was evaluated by measuring lactate dehydrogenase AU2 ▶ (LDH) release in media, using MTX-LDH kit (Kyokuto Pharm) in accordance with the manufacturer's instructions. ◀ AU3 Target cells (hADSCs/MSCs cultured with FBS, hADSCs/MSCs cultured with heat-inactivated NHS, or Panc02) were plated at a concentration of 1×10^4 cells/well in a 96-well culture plate. Then, DMEM with 20% or 40% fresh NHS was added. The plates were incubated for 2 h at 37°C, and LDH release was determined. All assays included maximal release controls (1% Triton X), controls with medium and target cells, with medium containing fresh NHS, and with medium alone.

Isolation of effector cells

Peripheral blood mononuclear cells (PBMCs) were isolated from the buffy coats from healthy volunteers using density gradient centrifugation with Lymphoprep (Nycomed). Cell viability was more than 98%, as determined by trypan blue exclusion. Human monocyte-derived macrophages were isolated and cultured as reported previously.[25]

ADCC assay

ADCC was also determined by measuring LDH release into medium. Target cells (hADSCs/MSCs cultured with FBS, hADSCs/MSCs cultured with heat-inactivated NHS, or Panc02) were plated in 96-well culture plates as described earlier. Then, 1×10^5 or 2×10^5 PBMCs in DMEM alone or with 10% heat-inactivated NHS were added. The plates were incubated for 4 h at 37°C, and LDH release was determined. All assays included maximal release controls (1% Triton X), controls with medium and target cells, with medium and effector cells, with medium containing 10% heat-inactivated NHS, and with medium alone.

Phagocytosis assay

Target cells (hADSCs/MSCs cultured with FBS, hADSCs/MSCs cultured with heat-inactivated NHS, or Panc02) were stained with PKH67 Green Fluorescent Cell Linker Mini Kit (Sigma Aldrich) according to the manufacturer's instructions. After labeling of target cells was terminated, the cells were washed and resuspended in RPMI medium. Then, 2×10^6 PKH67-labeled target cells were added into 24-well culture plates and incubated with 2×10^5 human

FIG. 2. Binding of natural preformed antibodies to hADSCs/MSCs. (**A**) Binding of natural preformed antibodies to Panc02 and hADSCs/MSCs. (**a**) Murine pancreatic carcinoma cell line Panc02 was exposed to 10% fresh NHS containing 15 mM EDTA, then stained with secondary FITC-conjugated goat anti-human IgG or IgM antibody, and studied by flow cytometry to demonstrate the binding of IgG and IgM. The natural performed antibodies human IgG and IgM bound onto Panc02. Exposition of Neu5Gc-preadsorbed NHS could reduce the natural performed antibody binding (IgG binding: 99.95% to 85.09%; IgM binding: 92.8% to 44.49%). (**b**) hADSCs/MSCs were cultured with FBS, exposed to 10% fresh NHS containing 15 mM EDTA, and then stained with secondary FITC-conjugated goat anti-human IgG or IgM antibody, or control goat IgG. The natural performed antibodies human IgG and IgM bound onto hADSCs/MSCs, and exposition of Neu5Gc-preadsorbed NHS could reduce IgG binding (80.01% to 2.08%). The percentage of cells that stained positive is indicated in the upper right corner of each panel. Data are representative of four independent experiments. (**B**) Anti-Neu5Gc antibody pretreatment suppressed the binding of natural preformed antibodies onto hADSCs/MSCs. hADSCs/MSCs cultured with FBS were precoated with anti-Neu5Gc antibody and then exposed to 10% fresh NHS containing 15 mM EDTA. The natural performed antibody human IgG bound onto hADSCs/MSCs, and exposition of anti-Neu5Gc antibody could reduce IgG binding (70.33% to 1.74%). The percentage of cells that stained positive is indicated in the upper right corner of each panel. Data are representative of three independent experiments. (**C**) Decrement of binding of natural preformed antibodies onto hADSCs/MSCs by chase with NHS. After cultivation of hADSCs/MSCs with heat-inactivated NHS but not FBS, the percentages of human IgG-positive cells decreased. The percentage of cells that stained positive is indicated in the upper right corner of each panel. Data are representative of four independent experiments. hADMSCs; EDTA, ethylenediaminetetraacetate; FITC, fluorescein isothiocyanate. ◀ AU5

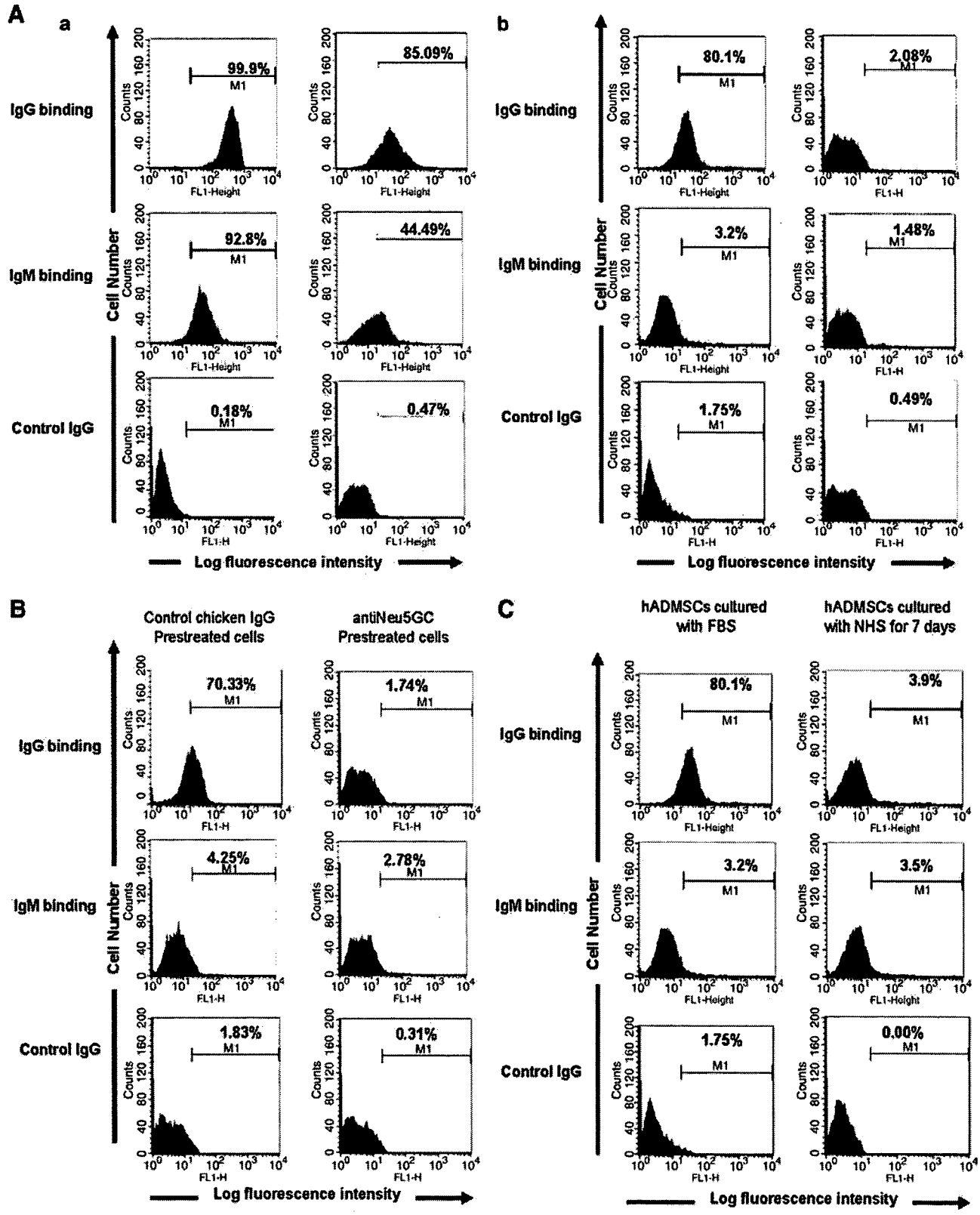
A
a
b
IgG binding
IgM binding
Control IgG
99.9%
85.09%
92.8%
44.49%
0.18%
0.47%
80.1%
2.08%
3.2%
1.48%
1.75%
0.49%
M1
Counts
FL1-Height
FL1-H
Cell Number
Log fluorescence intensity
B
Control chicken IgG
Prestreated cells
antiNeu5GC
Prestreated cells
70.33%
1.74%
4.25%
2.78%
1.83%
0.31%
C
hADMSCs cultured
with FBS
hADMSCs cultured
with NHS for 7 days
80.1%
3.9%
3.2%
3.5%
1.75%
0.00%

U5 ▶ monocyte-derived macrophages ($E{:}T = 1{:}10$) in 1 mL of RPMI 1640 medium alone or with 10% heat-inactivated NHS for 24 h at 37°C. Following incubation, the target cells and human monocyte-derived macrophages were harvested with EDTA solution. The cells were counterstained with allophycocyanin-conjugated mouse monoclonal antibodies to human CD11c (BD Pharmingen) and washed and fixed with 2% formaldehyde-PBS. Two-color flow cytometric analysis was performed with a FACSCalibur flow cytometer under optimal gating. PKH67-labeled target cells were detected in the FL-1 channel and allophycocyanin-labeled human monocyte-derived macrophages were detected in the FL-4 channel. Dual-labeled cells ($PKH67^+/CD11c^+$) were considered to represent phagocytosis of targets by human monocyte-derived macrophages. Residual target cells were defined as cells that were $PKH67^+/CD11c^+$.

Adipogenic and osteogenic differentiation procedure

For adipogenic differentiation, cells were cultured in differentiation medium (Zen-Bio). After 3 days, half of the medium was changed with adipocyte medium (Zen-Bio) every 2 days. Ten days after differentiation, characterization of adipocytes was confirmed by microscopic observation of intracellular lipid droplets by oil red O staining. Osteogenic differentiation was induced by culturing the cells in DMEM containing 10 nM dexamethasone, 50 mg/dL ascorbic acid 2-phosphate, 10 mM beta-glycerophosphate (Sigma), and 10% FBS or heat-inactivated NHS. The differentiation was examined by alizarin red staining and alkaline phosphatase (AP) activity. For alizarin red staining, 7 or 18 days after differentiation, the cells were washed three times and fixed with dehydrated ethanol. After fixation, the cells were stained with 1% alizarin red S in 0.1% NH_4OH (pH 6.5) for 5 min and then washed with H_2O. AP activity was investigated at 2 weeks after differentiation using the procedure described previously.[26] AP activity per cell was calculated based on the amount of DNA. DNA content was measured by a modification of the method of Labarca and Paigen.[27]

AU3 ▶ AU3 ▶

Statistics

Values are given as the mean ± standard deviation. Student's t-test was used to ascertain the significance of differences within groups. Differences were considered statistically significant when $p < 0.05$. All statistical analyses were performed using the SPSS Statistics 17.0 package (SPSS, Chicago, IL).

Results

Presence of Neu5Gc and human natural preformed antibodies binding to hADSCs/MSCs

First, the specificity of chicken anti-Neu5Gc polyclonal antibody was examined (Fig. 1A). Flow cytometric analysis showed that chicken anti-Neu5Gc polyclonal antibody bound to the surfaces of Panc02, which constitutively expressed Neu5Gc, but Neu5Gc-preadsorbed anti-Neu5Gc polyclonal antibody could not react, indicating the anti-Neu5Gc antibody reacts to Neu5Gc specifically. Next, incorporation of Neu5Gc antigen via FBS-containing medium was examined (Fig. 1B). Fresh hADSCs/MSCs did not express Neu5Gc on their cell surface. In accordance with passage numbers, the population of Neu5Gc-positive cells has increased by cultivation with FBS (fresh: 0.33%; passage number 2: 19.77%; and passage number 5: 86.6%). Culture with heat-inactivated NHS could markedly reduce Neu5Gc in human colon carcinoma cells,[22] hESCs,[13] and hMSCs,[14] apparently as the result of metabolic replacement by *N*-acetylneuraminic acid in the human serum. So, the reduction of incorporated Neu5Gc xenoantigen by chasing cultivation with human serum was examined (Fig. 1C). The Neu5Gc xenoantigen was reduced after cultivation of hADSCs/MSCs with heat-inactivated NHS but not FBS. The percentages of Neu5Gc-positive cells have decreased in accordance with culture duration, and the decrement manners of second passaged hADSCs/MSCs and fifth passaged ones have been in a similar fashion.

F1 ▶

Because human serum contains high titers of natural preformed antibodies against the Neu5Gc xenoantigen,[20–22] we assessed whether such antibodies could recognize Neu5Gc-containing epitopes on hADSCs/MSCs cultured with FBS (Fig. 2). Panc02 cultured with FBS and exposed to 10% fresh NHS containing 15 mM EDTA showed high human IgG (99.9%) and IgM (92.8%) binding (Fig. 2Aa). hADSCs/MSCs cultured with FBS and treated with fresh NHS also showed high human IgG binding (80.1%), but human IgM binding was very low (3.2%) (Fig. 2Ab). Preincubation of fresh NHS with Neu5Gc resulted in significant decrease in human IgG binding on hADSCs/MSCs cultured with FBS (80.1% to 2.08%). Further, pretreatment of hADSCs/MSCs with anti-Neu5Gc polyclonal antibody also resulted in reduction of human IgG binding (70.33% to 1.74%; Fig. 2B). Culturing hADSCs/MSCs with heat-inactivated NHS, which decreased Neu5Gc expression of hADSCs/MSCs effectively, reduced human IgG binding on hADSCs/MSCs when exposed to fresh NHS (Fig. 2C). Taken together, these data indicate that the hADSCs/MSCs cultured with FBS expressed Neu5Gc and the human natural preformed antibodies could bind to hADSCs/MSCs. This binding of human natural preformed antibodies on hADSCs/MSCs was related to the amount of Neu5Gc on hADSCs/MSCs. Culture with heat-inactivated NHS could markedly reduce IgG binding on hADSCs/MSCs when exposed to fresh NHS (80.1% to 3.9%).

◀ F2

Complement fragment deposition on hADSCs/MSCs and CMC assay

Cell surface antibody binding may activate the classical complement pathway leading to cytotoxicity. We assessed whether the deposition of complement fragments on hADSCs/MSCs occurred after exposure to fresh NHS. Whether hADSCs/MSCs were cultured with FBS or heat-inactivated NHS, the amount of deposition of C4 and C3 fragments on hADSCs/MSCs after a short incubation period of 30 min was no different from negative control (cells incubated with DMEM alone or 10% fresh NHS in DMEM containing 15 mM EDTA) (Fig. 3). To control for fresh NHS activity and variability, we tested the deposition of C4 and C3 fragments on Panc02. Both complement fragments were clearly deposited on Panc02 (C4: 84.6%; C3: 98.99%) and this deposition was abolished by adding 15% EDTA (Fig. 3). We next analyzed the CMC of hADSCs/MSCs cultured with FBS or heat-inactivated NHS. To control for CMC of fresh NHS, we tested CMC of Panc02. CMC of Panc02 was clearly detected (20% NHS: 42.7% ± 4.7%; 40% NHS: 65.4% ± 2.4%).

◀ F3

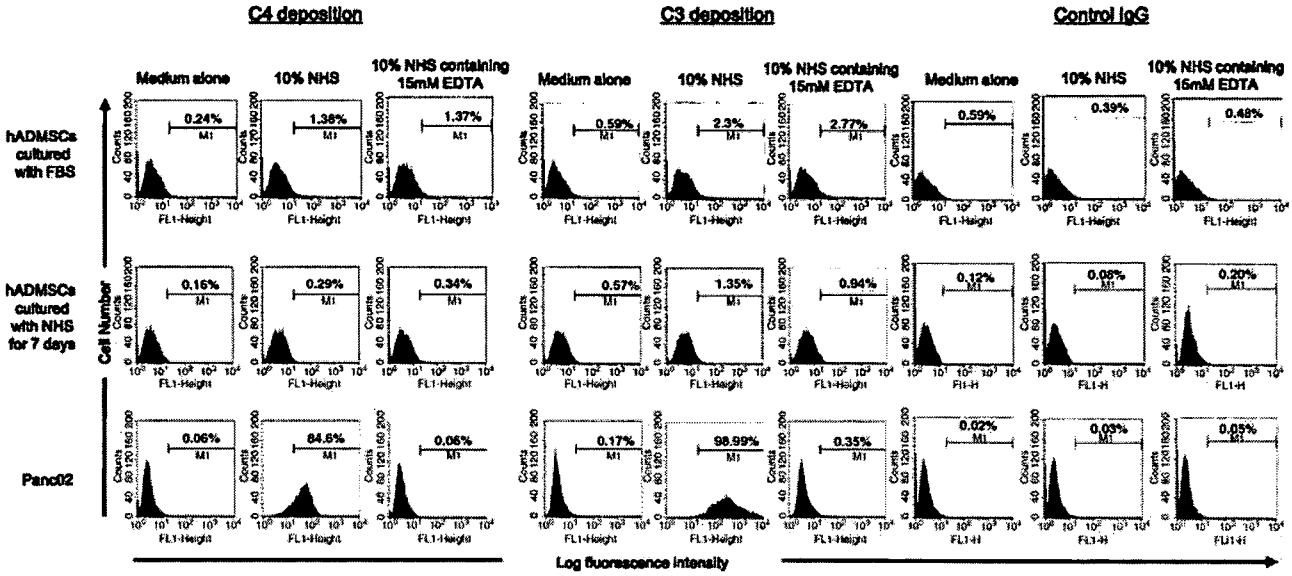

FIG. 3. Complement deposition onto hADSCs/MSCs by NHS. The cells were exposed to medium alone, 10% NHS, or 10% NHS containing 15 mM EDTA, followed by an analysis of deposition of complement fragments C4 and C3. The percentage of cells that stained positive is indicated in the upper right corner of each panel. Data are representative of four independent experiments.

In contrast, significant specific lysis of hADSCs/MSCs cultured with FBS or heat-inactivated NHS was not detected (hADSCs/MSCs cultured with FBS + 20% NHS: 4.8% ± 1.3%; or 40% NHS: 7.4% ± 2.0%; hADSCs/MSCs cultured with heat-inactivated NHS: 20% NHS: 3.6% ± 1.6%; 40% NHS: 5.6% ± 1.6%). We then analyzed the expression of complement regulatory proteins such as CD46, CD55, and CD59 on hADSCs/MSCs. hADSCs/MSCs were weakly positive for both CD46 (22.1%) and CD55 (29.8%) and highly positive for CD59 (97.5%) (Fig. 4B). These data indicate that hADSCs/MSCs express complement regulatory proteins such as CD46, CD55, and CD59 and are largely resistant to killing by CMC mechanism.

F4 ▶

ADCC of hADSCs/MSCs mediated by human natural preformed antibodies in NHS

IgG antibodies play an important role in ADCC.[28] Our study demonstrated that natural preformed IgG antibodies could bind to hADSCs/MSCs cultured with FBS. Therefore, to evaluate the role of these IgG antibodies in cell-mediated cytotoxicity, ADCC assay was performed with hADSCs/MSCs cultured with FBS, hADSCs/MSCs cultured with heat-inactivated NHS, or Panc02 as targets and human PBMCs as effector cells, using *E:T* ratios of 10:1 and 20:1, and 4-h incubation periods. PBMCs in the absence of heat-inactivated NHS caused no significant lysis of hADSCs/MSCs cultured with FBS, hADSCs/MSCs cultured with heat-inactivated NHS, and Panc02 (hADSCs/MSCs cultured with FBS: *E:T* = 10:1, 2.37% ± 0.35%; *E:T* = 20:1, 3.78% ± 0.85%; hADSCs/MSCs cultured with heat-inactivated NHS: *E:T* = 10:1, 0.57% ± 0.36%; *E:T* = 20:1, 2.34% ± 0.67%; Panc02: *E:T* = 10:1, 1.98% ± 0.35%; *E:T* = 20:1, 4.7% ± 0.54; Fig. 5, white bar). The cytotoxicity of Panc02 in the presence of heat-inactivated NHS was significantly greater than that in the absence of heat-inactivated NHS (in the presence of NHS vs. in the absence of heat-inactivated NHS: *E:T* = 10:1, 27.4% ± 3.1% vs. 1.98% ± 0.35%, $p < 0.05$; *E:T* = 20:1, 28.9% ± 4.6% vs. 4.7 ± 0.54%, $p < 0.05$), which proved the effective use of PBMCs (Fig. 5). A significant increase of cytotoxicity of the hADSCs/MSCs cultured with FBS was also evident in the presence of heat-inactivated NHS (in the presence of heat-inactivated NHS vs. in the absence of heat-inactivated NHS: *E:T* = 10:1, 13.5% ± 0.82% vs. 2.37% ± 0.35%, $p < 0.05$; *E:T* = 20:1, 16.0% ± 1.5% vs. 3.78% ± 0.85, $p < 0.05$; Fig. 5). In contrast, no increase of cytotoxicity of the hADSCs/MSCs cultured with heat-inactivated NHS was detected in the presence of heat-inactivated NHS (in the presence of heat-inactivated NHS vs. in the absence of heat-inactivated NHS: *E:T* = 10:1, 3.23% ± 0.52% vs. 0.57% ± 0.36%; *E:T* = 20:1, 3.75% ± 0.51% vs. 2.34% ± 0.67%; Fig. 5). In addition, the cytotoxicity the hADSCs/MSCs cultured with FBS was significantly greater than that of hADSCs/MSCs cultured with heat-inactivated NHS which expressed negligible amount of Neu5Gc (hADSCs/MSCs cultured with FBS vs. hADSCs/MSCs cultured with heat-inactivated NHS: *E:T* = 10:1, 13.5% ± 0.82% vs. 3.23% ± 0.52%, $p < 0.05$; *E:T* = 20:1, 16.0% ± 1.5% vs. 3.75% ± 0.51, $p < 0.05$; Fig. 5). Taken together, these data indicate that the hADSCs/MSCs cultured with FBS are injured by ADCC mechanism. In contrast, hADSCs/MSCs cultured with NHS are less sensitive to ADCC.

F5 ▶

Phagocytosis of hADSCs/MSCs by human monocyte-derived macrophages

hADSCs/MSCs cultured with FBS, hADSCs/MSCs cultured with heat-inactivated NHS, or Panc02 were stained with fluorescent PKH67, respectively. Labeled cells were cocultured with human monocyte-derived macrophages in the presence or absence of heat-inactivated NHS for 24 h. After counterstaining with monoclonal antibodies to human CD11c, two-color flow cytometric analysis was performed

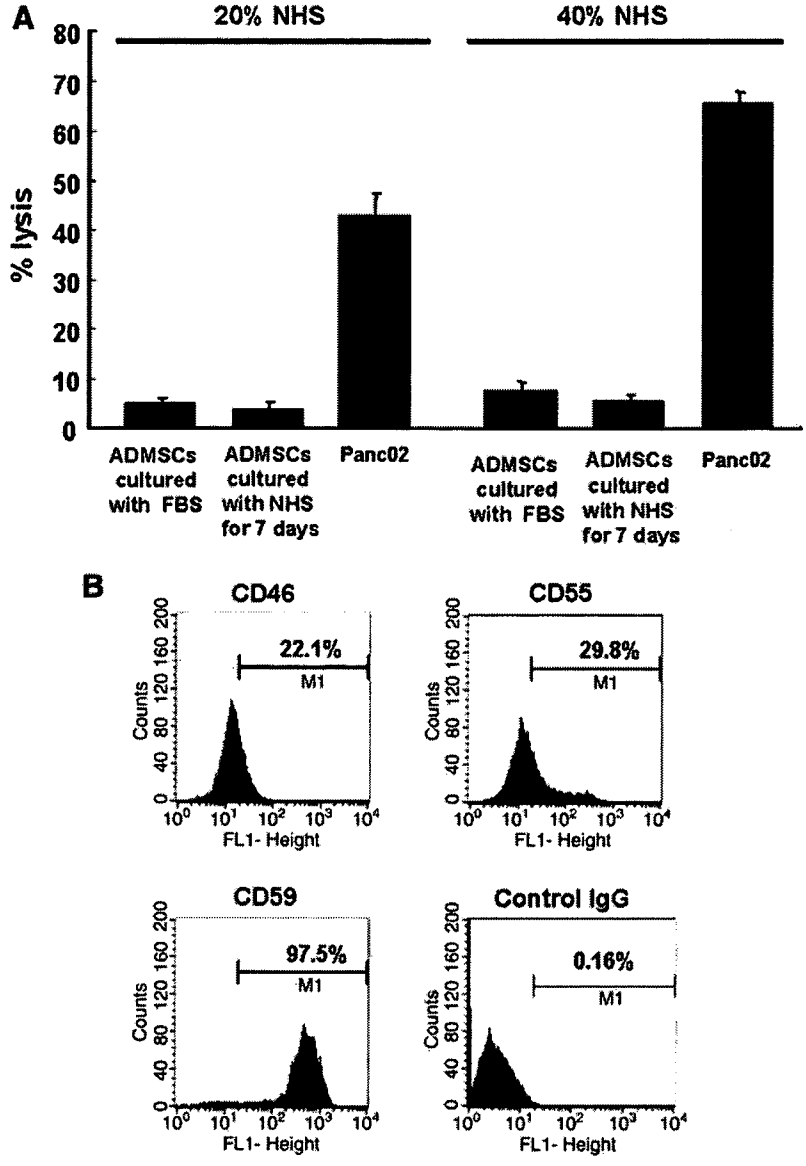

FIG. 4. Sensitivity of hADMSCs to lysis by NHS. (**A**) Complement-mediated cytotoxicity assay of hADSCs/MSCs. The cytotoxic activity of 20% or 40% NHS against hADSCs/MSCs was tested by lactate dehydrogenase release. Data are shown as mean ± standard deviation. (**B**) Complement regulatory proteins on hADSCs/MSCs were studied by flow cytometry using FITC-conjugated antibodies to human CD46, CD55, CD59, or control IgG. Data are representative of three independent experiments.

F6 ▶ (Fig. 6). Phagocytosis of target cells by human monocyte-derived macrophages could be identified as dual-labeled cells (PKH67$^+$/CD11c$^+$, right upper panel). Similar results were obtained in three independent experiments. Phagocytosis of Panc02 was clearly detectable (10.6%) and increased twofold in the presence of heat-inactivated NHS, which proved the effective use of human monocyte-derived macrophages. Phagocytosis of hADSCs/MSCs cultured with NHS by human monocyte-derived macrophages was somewhat detectable (5.7%) and also increased in the presence of heat inactivated human serum (9.3%). In contrast, human monocyte-derived macrophages could not phagocytose hADSCs/MSCs cultured with heat-inactivated NHS neither in the absence nor in the presence of heat-inactivated NHS (medium alone: 1.1%; 10% heat-inactivated NHS: 2.2%; Fig. 6). Thus, human monocyte-derived macrophages phagocytosed hADSCs/MSCs cultured with FBS and this phagocytic activity increased when hADSCs/MSCs cultured with FBS were opsonized by the natural preformed antibodies in the presence of heat-inactivated NHS. In contrast, hADSCs/MSCs cultured with heat-inactivated NHS were resistant to phagocytosis either in the absence or in the presence of heat-inactivated NHS.

Adipogenic and osteogenic differentiation potentials of hADSCs/MSCs cultured with FBS and heat-inactivated NHS

To compare the *in vitro* differentiation potential of hADSCs/MSCs cultured with FBS or heat-inactivated NHS, cells were differentiated toward the adipogenic and osteogenic lineages. Adipogenic differentiation was induced by culture with differentiation medium containing 1-methyl-3-isobutylxanthine, PPAR-gamma agonist, dexamethasone, and insulin. The acquisition of the adipogenic phenotype was determined by staining the cell monolayers with oil red O (Fig. 7A). The efficiency of adipogenesis of hADSCs/MSCs cultured with heat-inactivated NHS was similar to that of hADSCs/MSCs cultured with FBS (Fig. 7A). Both hADSCs/MSCs showed multiple intracellular lipid-filled droplets in 35–50% of cells

◀ AU2

◀ F7

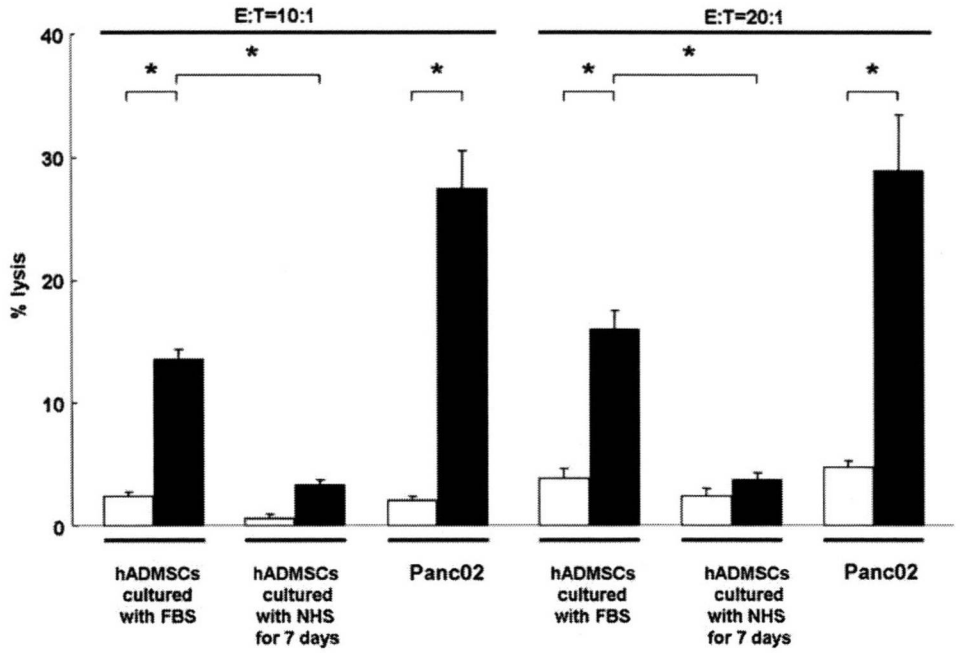

FIG. 5. Antibody-dependent cell-mediated cytotoxicity assay of hADSCs/MSCs. The cytotoxic activity of peripheral blood mononuclear cells against hADSCs/MSCs in the absence (white bar) or presence (black bar) of 10% NHS was tested by measuring lactate dehydrogenase release into medium ($E{:}T = 10{:}1$ or 20:1). Data are shown as mean ± standard deviation ($^*p < 0.05$) and are representative of three independent experiments. ◀AU2

after adipogenic induction. Osteogenic differentiation was induced by treating cells with low concentrations of dexamethasone, ascorbic acid, and beta-glycerophosphate. Calcium deposition was demonstrated by staining monolayers with alizarin red (Fig. 7B). hADSCs/MSCs cultured with heat-inactivated NHS and those cultured with FBS showed similar potential toward osteogenic differentiation. High AP activity was detected in hADSCs/MSCs cultured with heat-inactivated NHS and those cultured with FBS in response to osteogenic induction after 2 weeks (Fig. 7B).

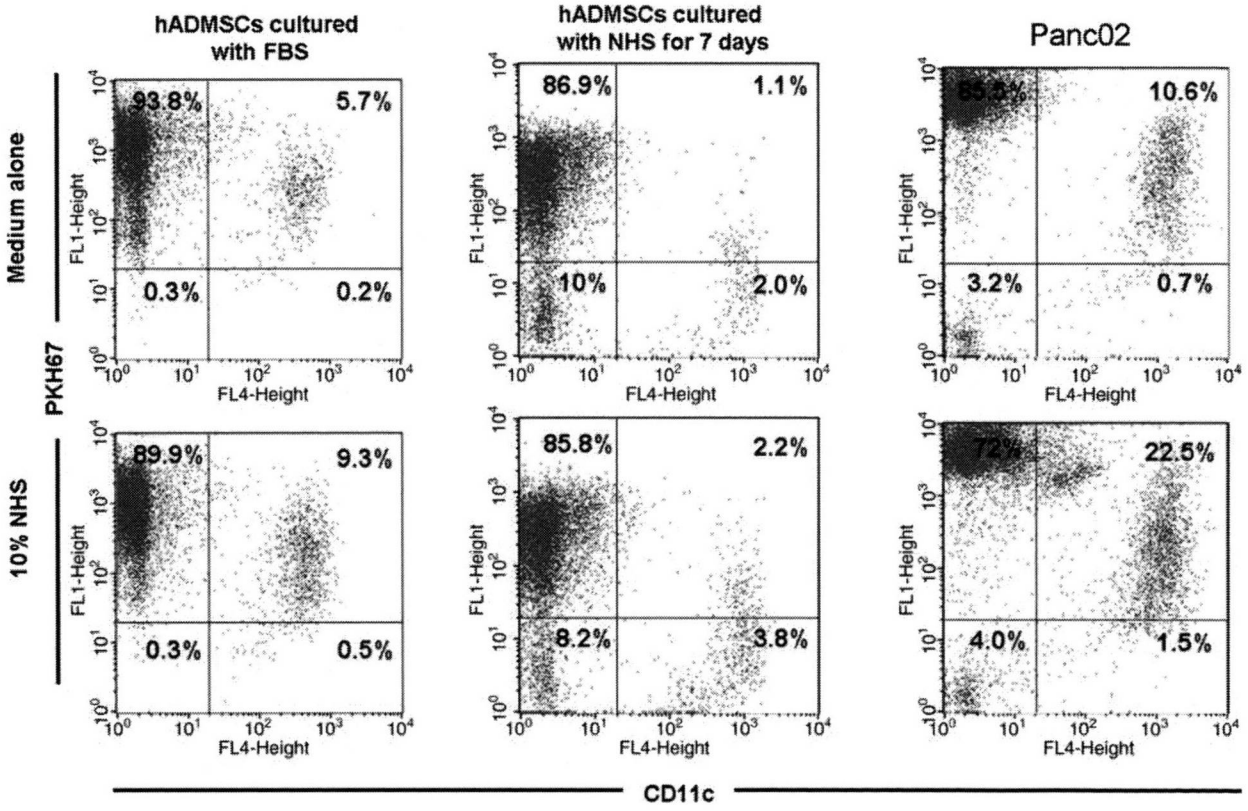

4C▶

FIG. 6. Representative flow cytometry profiles of phagocytosis assay of hADSCs/MSCs. Upper left quadrant: Region of residual target cells. Upper right quadrant: Region of phagocytosed target cells. Percentages represent those of total cells in each region. Data are representative of three independent experiments.

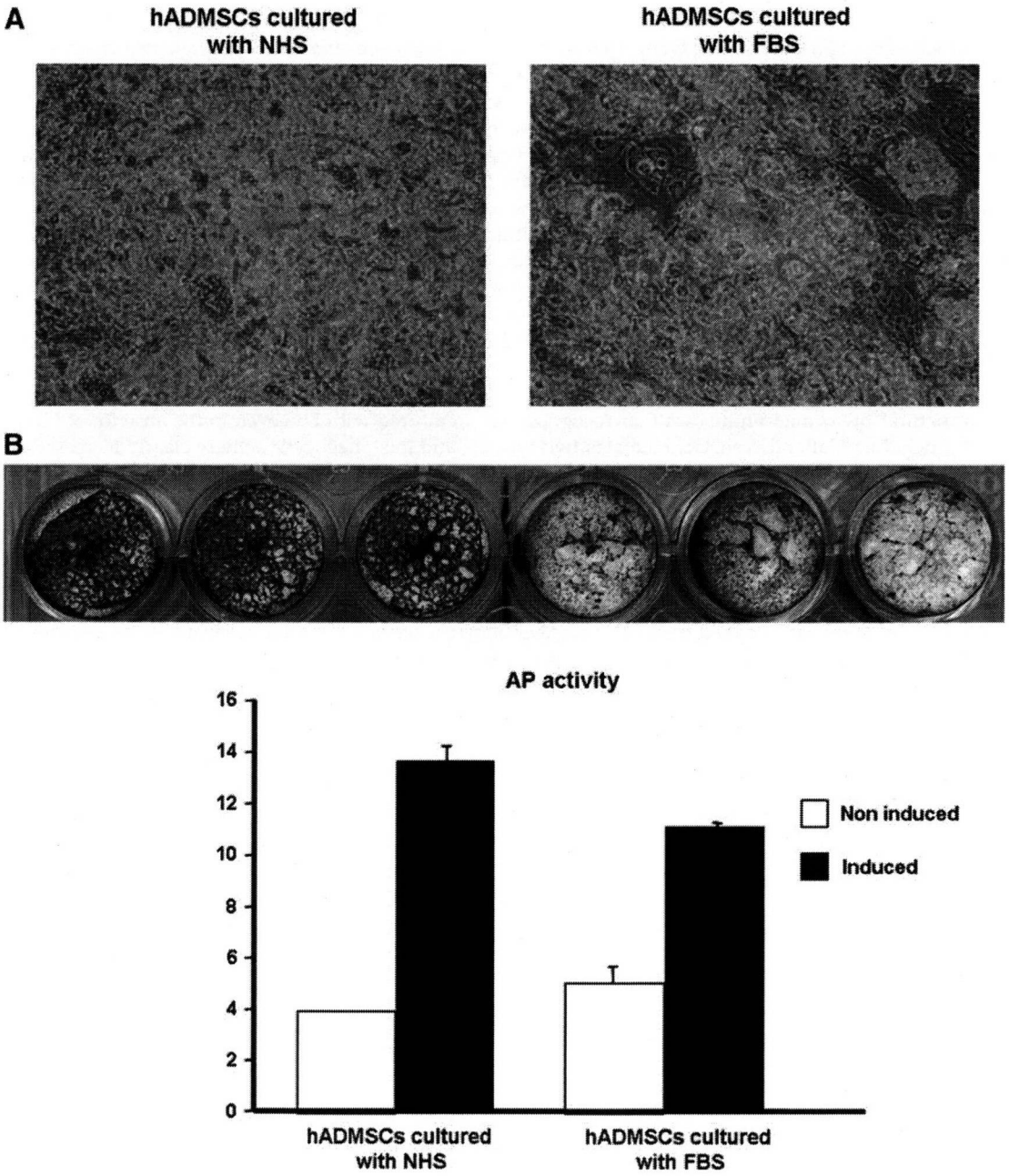

FIG. 7. Adipogenic and osteogenic differentiation potentials of hADSCs/MSCs cultured with FBS and NHS. (**A**) The efficiency of adipogenesis of hADSCs/MSCs cultured with NHS was similar to that of hADSCs/MSCs cultured with FBS. (**B**) The efficacy of osteogenic differentiation and alkaline phosphatase activity was similar between cultures with NHS and FBS in response to osteogenic induction. Data are representative of four independent experiments.

Discussion

Previous studies have reported that hESCs and BM-derived hMSCs are capable of efficient Neu5Gc uptake from culture media components.[13,14] Human serum contains high titers of natural preformed antibodies against Neu5Gc xenoantigen[20–22] and binding of these natural preformed antibodies may lead to immune responses. Importantly, this may be reflected in the published results of human clinical trials using BM-derived hMSCs cultured with FBS.[8–12] Further, in human clinical trials with FBS-grown hMSCs, antibodies against FBS have been detected.[12] However, these immune responses against human stem cells mediated by natural preformed antibodies remain in controversary.[13,23] In this study, because of the usefulness of hADSCs/MSCs as an alternative source of stem cells, we assessed the presence of Neu5Gc in hADSCs/MSCs cultured with FBS and the human immune response mediated by Neu5Gc xenoantigen.

Our study using a chicken anti-Neu5Gc polyclonal antibody showed that most of the hADSCs/MSCs cultured with FBS expressed Neu5Gc xenoantigen. This result is similar to the previous study that hESCs and BM-derived hMSCs express Neu5Gc.[13,14] In addition, our data suggested